

# A Spitzer Study of Debris Disks In The Young Nearby Cluster NGC 2232: Icy Planets Are Common Around $\sim 1.5\text{--}3\text{ M}_{\odot}$ Stars

Thayne Currie<sup>1</sup>, Peter Plavchan<sup>2</sup>, and Scott J. Kenyon<sup>1</sup>

tcurrie@cfa.harvard.edu, plavchan@ipac.caltech.edu, skenyon@cfa.harvard.edu

## ABSTRACT

We describe Spitzer IRAC and MIPS observations of the nearby 25 Myr-old open cluster NGC 2232. Combining these data with ROSAT All-Sky Survey observations, proper motions, and optical photometry/spectroscopy, we construct a list of highly probable cluster members. We identify 1 A-type star, HD 45435, with definite excess emission at  $4.5\text{--}24\text{ }\mu\text{m}$  indicative of debris from terrestrial planet formation. We also identify 2–4 late-type stars with possible  $8\text{ }\mu\text{m}$  excesses, and 8 early-type stars with definite  $24\text{ }\mu\text{m}$  excesses. Constraints on the dust luminosity and temperature suggest that the detected excesses are produced by debris disks. From our sample of B and A stars, stellar rotation appears correlated with  $24\text{ }\mu\text{m}$  excess, a result expected if massive primordial disks evolve into massive debris disks. To explore the evolution of the frequency and magnitude of debris around A-type stars, we combine our results with data for other young clusters. The frequency of debris disks around A-type stars appears to increase from  $\sim 25\%$  at 5 Myr to  $\sim 50\text{--}60\%$  at 20–25 Myr. Older A-type stars have smaller debris disk frequencies:  $\sim 20\%$  at 50–100 Myr. For these ages, the typical level of debris emission rises from 5–20 Myr and then declines. Because  $24\text{ }\mu\text{m}$  dust emission probes icy planet formation around A-type stars, our results suggest that the frequency of icy planet formation is  $\eta_i \gtrsim 0.5\text{--}0.6$ . Thus, most A-type stars ( $\approx 1.5\text{--}3\text{ M}_{\odot}$ ) produce icy planets.

*Subject headings:* stars: pre-main-sequence– planetary systems: formation, planetary systems: protoplanetary disks, Infrared: Stars, Galaxy: Open Clusters and Associations: Individual: NGC Number: NGC 2232, stars: individual (HD 45435)

---

<sup>1</sup>Harvard-Smithsonian Center for Astrophysics, 60 Garden St. Cambridge, MA 02140

<sup>2</sup>Michelson Science Center, M/C 100-22, California Institute of Technology, 770 S. Wilson Ave., Pasadena, CA 91125

## 1. Introduction

Recent studies of young stellar clusters from the *Spitzer Space Telescope* (Werner et al. 2004) provide powerful insights into the emergence of mature planetary systems from primordial disks surrounding young stars. Spitzer observations indicate that the initial stages of primordial disk evolution proceed rapidly. Within  $\sim 1\text{--}3$  Myr, many optically-thick primordial disks undergo dust settling, form inner regions cleared of dust, and undergo grain growth to sizes larger than the sub-micron sizes characteristic of the interstellar medium (e.g. Calvet et al. 2005; Lada et al. 2006; Sargent et al. 2006; Bouwman et al. 2008). As these processes occur, the level of inner disk emission drops and the frequency of primordial disks declines (e.g. Hernandez et al. 2007, see also Hillenbrand 2005). Primordial disks around early type stars disappear faster than around later-type stars (Carpenter et al. 2006; Hernandez et al. 2007; Currie and Kenyon 2008).

By  $\sim 10\text{--}15$  Myr, primordial disks are exceedingly rare. The disk population is then dominated by optically thin, gas-poor *debris disks* (Hernandez et al. 2006; Currie et al. 2007a; Currie and Kenyon 2008). Because debris dust is removed on timescales much shorter than the age of the star, the dust must be replenished to sustain disk emission. Collisions between  $\gtrsim$  km-sized planetesimals excited by large-scale planet formation (e.g. Backman and Paresce 1993; Kenyon and Bromley 2004) can provide this replenishment. Though debris disks around early-type stars can appear as soon as  $\sim 3$  Myr (Currie and Kenyon 2008), the mid-IR debris emission does not peak until  $\approx 10\text{--}20$  Myr (Currie et al. 2008a). This rise in debris emission is consistent with planetesimal collisions during the growth of icy protoplanets in the outer disk (Kenyon and Bromley 2008). After protoplanets reach their maximum size at  $\approx 20\text{--}30$  Myr, the level of debris emission decays as  $\sim t^{-1}$  (Rieke et al. 2005; Su et al. 2006). This decay is consistent with steady-state collision models (e.g. Wyatt et al. 2007).

The epoch of maximum debris emission ( $\sim 10\text{--}30$  Myr) is also important for terrestrial planet formation. Planet formation models and radiometric dating suggest that terrestrial planets reach their final mass by  $\sim 10\text{--}30$  Myr (Wetherill and Stewart 1993; Yin et al. 2002; Kenyon and Bromley 2006). Terrestrial planet formation produces debris emission observable at  $\approx 5\text{--}10\ \mu\text{m}$ . Mid-IR Spitzer observations reveal terrestrial zone dust emission around many 13 Myr old stars in the massive Double Cluster,  $\eta$  and  $\chi$  Persei, and several stars in other  $\lesssim 40$  Myr old clusters/associations including Sco-Cen, NGC 2547, and the  $\beta$  Pic Moving Group (Zuckerman and Song 2004; Chen et al. 2005a, 2006; Currie et al. 2007b; Rhee et al. 2007b; Gorlova et al. 2007; Currie et al. 2008a; Lisse et al. 2008)<sup>1</sup>. Observations of many

---

<sup>1</sup>At least two other, much older stars harbor warm debris disks that may be indicative of stochastic collisions in the terrestrial zone: BD +20° 307 and HD 23514 (Song et al. 2005; Rhee et al. 2008)

warm, IRAC-excess stars in  $\eta$  and  $\chi$  Persei point to a spectral-type/stellar-mass dependent evolution of terrestrial zone dust, suggesting that the terrestrial planet formation process runs to completion faster for high-mass stars than for intermediate-mass stars (Currie et al. 2007a; Currie 2008).

Reconstructing the time history of terrestrial and icy planet formation at the 10–40 Myr epoch requires Spitzer IRAC and MIPS observations of many clusters besides  $\eta$  and  $\chi$  Persei. While observations of stars in 10–20 Myr old Sco-Cen and the  $\beta$  Pic moving group provide important studies of cold dust probed by MIPS (Chen et al. 2005a; Rebull et al. 2008), strong constraints on warm dust probed by  $\leq 10$ – $15\ \mu\text{m}$  broadband photometry of cluster members are limited to IRAS, MSX, and ground-based campaigns with much poorer sensitivity. The FEPS (*Formation and Evolution of Planetary Systems*; Meyer et al. 2006) Legacy Program observed  $\sim 35$  10–20 Myr-old Sco-Cen sources in IRAC with a range of spectral types ( $\sim$  F8/G0 to K3). However, this sample size is too small to provide statistically robust constraints given the low overall frequency of warm dust emission (Mamajek et al. 2004; Currie et al. 2007a; Gorlova et al. 2007).

Though  $\eta$  and  $\chi$  Persei is massive enough to investigate the frequency of warm dust from terrestrial planet formation in one environment, observations of other clusters are needed to constrain the time evolution of warm dust in many environments. The Spitzer survey of NGC 2547 (Gorlova et al. 2007) potentially fill this void in sampling, yielding a large population of cluster stars ( $\sim 400$ – $500$ ) and revealing warm dust around at least  $\sim 6$  FGKM stars. However, recent work has revised the age of NGC 2547 upward from 25 Myr to  $\sim 35$ – $40$  Myr (Naylor and Jeffries 2006; Mayne and Naylor 2008). Spitzer studies of other  $\sim 15$ – $35$  Myr-old clusters would then clearly aid in constraining the evolution of the observable signatures of terrestrial planet formation.

Understanding the evolution of cold dust emission from debris disks also requires additional observations of 15–35 Myr-old clusters. While  $24\ \mu\text{m}$  debris disk emission around early-type stars peaks at  $\approx 10$ – $20$  Myr, the evolution of debris emission at  $\approx 20$ – $30$  Myr is not well constrained. Few clusters in this age range have been observed with Spitzer. The most populous cluster previously assigned to this age range, NGC 2547, is likely older. Observing 20–30 Myr old clusters may also reveal a delay in the peak debris emission for later type, lower-mass stars relative to early-type stars as implied by planet formation models (e.g. Kenyon and Bromley 2008). Observations of young stars at  $70\ \mu\text{m}$  may provide tentative evidence for this delay (Hillenbrand et al. 2008). Furthermore, the disk environment around late type, low-mass stars may be qualitatively different due to the importance of corpuscular wind drag in removing debris dust (Plavchan et al. 2005). Recent Spitzer studies argue that detectable debris disks around M stars may be rarer than around intermediate/high-mass

stars (Gautier et al. 2007; Plavchan et al. 2008). To further investigate this possibility, MIPS observations of M dwarf stars provide new constraints on planet formation processes.

In this paper, we investigate debris disk evolution and planet formation in the young open cluster NGC 2232 located in Gould’s Belt close to the Orion Nebula Cluster. Until very recently, the most complete studies of this cluster date from over 30 years ago (Claria 1972; Levato and Malaroda 1974), which identify NGC 2232 as a group of proper motion stars with B-F spectral types and an age of  $\sim 20$ –25 Myr. Based on pre-main sequence evolutionary models, Lyra et al. (2006) estimate an age of 25–30 Myr and find a 25 Myr nuclear age. Both Claria (1972) and Lyra et al. (2006) show that the cluster is nearby ( $\sim 320$ –360 pc). At this distance, IRAC observations can probe well into the M dwarf regime; MIPS observations can detect the photospheres of early and intermediate-mass stars. The cluster has an extremely low mean reddening ( $E(B-V) \sim 0.07$ ; Lyra et al. 2006). Thus, NGC 2232’s distance, age, and reddening combine to make investigating debris disk evolution feasible in a way that complements previous studies of  $\eta$  and  $\chi$  Persei and NGC 2547.

Our investigation is organized as follows. After describing the observations, image processing, and photometry of Spitzer IRAC/MIPS sources, we match sources with 2MASS/optical VI data in §2. Analysis of these sources shows that many may have excess emission from circumstellar dust. To identify cluster members, we rely on ROSAT x-ray observations, proper motion data, optical/IR color-magnitude diagrams and spectroscopy in §3. In §4 and 5, we analyze Spitzer data of x-ray selected cluster members to identify stars with evidence for circumstellar dust, identify stars with active terrestrial planet formation, and explore any statistical trends in the disk population with the stellar properties and in the level of debris emission with time.

NGC 2232 harbors a substantial population of stars with  $24\ \mu m$  excess with a range of spectral types from late B to late K spectral type. At least one star (HD 45435) shows evidence for warm  $8\ \mu m$  excess. Constraining the disk luminosity and dust temperature of this source and comparing its SED to debris disk models shows that its warm dust emission is plausibly produced by terrestrial planet formation.

This survey yields robust constraints on the evolution of cold debris disks. We identify a correlation between stellar rotation and  $24\ \mu m$  excess for high-mass stars that may reveal an evolutionary link between massive primordial disks and massive debris disks. When combined with Spitzer data of other young clusters, our survey shows that the level of debris emission around A stars in the cluster is consistent with a peak in the  $24\ \mu m$  debris emission at  $\sim 10$ –20 Myr, confirming the results of recent surveys (Currie et al. 2008a). The frequency of  $24\ \mu m$  debris emission *increases* from  $\sim 5$  Myr and peaks between 10 Myr and 30 Myr.

Finally, this work has important implications for the frequency of icy planets around high-mass, early-type stars. The fraction of A stars ( $\approx 1.5\text{--}3\text{ M}_{\odot}$ ) with  $24\text{ }\mu\text{m}$  excess emission is high ( $\geq 50\%$ ). Because this emission likely comes from disk regions beyond the ice line ( $\approx 170\text{ K}$ ), these results imply that icy planets around A stars are common.

## 2. Data

### 2.1. Spitzer IRAC and MIPS photometry

#### 2.1.1. Observations and Image Processing

Observations of NGC 2232 were taken with the Infrared Array Camera (IRAC; Fazio et al. 2004) and Multiband Imaging Photometer for Spitzer (MIPS; Rieke et al. 2004) on March 29, 2005 and April 4, 2005 as a part of the *Guaranteed Time Observations* program (Program ID 37). Both sets of data for NGC 2232 ( $l = 215^{\circ}$ ,  $b = -7.4^{\circ}$ ) cover  $\sim 1.4$  square degrees on the sky with boundaries of  $\alpha_{2000} \sim 6^{\text{h}}25^{\text{m}}50^{\text{s}} - 6^{\text{h}}30^{\text{m}}00^{\text{s}}$  and  $\delta_{2000} \sim -5^{\circ}30^{\text{m}}00^{\text{s}} - -4^{\circ}05^{\text{m}}00^{\text{s}}$ . The IRAC observations consist of high-dynamic range exposures of 0.6s and 10.4s at  $3.6\text{ }\mu\text{m}$ ,  $4.5\text{ }\mu\text{m}$ ,  $5.8\text{ }\mu\text{m}$ , and  $8\text{ }\mu\text{m}$ . Sources were typically observed at four dither points, which yielded an average integration time/pixel of  $\sim 2.4\text{ s}$  and  $41.6\text{ s}$  for the short and long exposures. The integration time/pixel was less for the edges of the region ( $\sim 20.8\text{ s}$ ) and more for central regions where dithered images overlap. The MIPS observations at  $24\text{ }\mu\text{m}$  and  $70\text{ }\mu\text{m}$  were taken in scan mode with a typical integration time/pixel of 80s. Background cirrus levels are low ( $\sim 28\text{ MJy/sr}$ ) and vary little ( $\sim 3\%$ ) across the MIPS field.

While the MIPS Basic Calibration Data (BCD) are largely free of artifacts, the IRAC BCD data require additional post-BCD processing before mosaicing. Using a custom IDL script written by T. C., we applied the appropriate array-dependent correction for point sources on each IRAC BCD frame (Quijada et al. 2004). Inspection of the 10.4s BCD frames showed that many bright stars produce severe ‘striping’ and column pulldown effects, especially in the [3.6] and [4.5] channels. For columns with bright stars, column pulldown shifts the background flux levels by up to  $\sim 2\text{ MJy/sr}$ . We removed these artifacts by applying a modified version of the *muxstriping* and *column pulldown* algorithms developed by Jason Surace and Leonidas Moustakas available on the *Spitzer Science Center* website. These steps drastically reduce striping and bias level artifacts. Flux levels for stars change by up to  $\sim 5\text{--}10\%$  in all channels due to the array-dependent correction and up to 30% for faint stars in channels 1 and 2 in columns affected by bright stars.

We then processed both the IRAC and MIPS data with the MOPEX/APEX pipeline,

interpolating over bad pixels. Using a bicubic interpolation with outlier rejection, the individual processed BCD frames were combined together into a single image in each filter for each exposure time. The final mosaics were inspected and cleared of any remaining image artifacts or pattern noise that could seriously compromise the photometry.

### 2.1.2. Photometry

Because the IRAC data are not well sampled (except for the brightest stars) and the point-spread function core is poorly characterized, we performed source finding and aperture photometry with a combination of SExtractor (Bertin and Arnouts 1996) and IDLPHOT routines in lieu of PRF fitting with APEX. For source identification with SExtractor, we constructed a background map for each IRAC mosaic in a 24x24 pixel area smoothed by an 8x8 pixel box. Sources were identified by their fluxes relative to the standard deviation in the background rms ( $\sigma_{bkgd,rms}$ ). Groups of pixels with counts greater than  $5\sigma_{bkgd,rms}$  ( $2\sigma_{bkgd,rms}$ ) were identified as sources for the [3.6] and [4.5] ([5.8] and [8]) filters. The resulting source lists were used as input for aperture photometry with the *aper.pro* routine. The source flux was computed in a 2 ( $\sim 2.44''$ ) and 3 pixel ( $\sim 3.66''$ ) aperture radius, using a local background calculated from a 4 pixel-wide annulus surrounding each source extending from 2-6 and 3-7 pixels. We multiplied the source fluxes by the appropriate aperture corrections from the IRAC data handbook, version 3.0<sup>2</sup>. To fine-tune the aperture correction, we compared the photometry for the brightest unsaturated sources derived above with that using a 10 pixel aperture, which should require no aperture correction.

Photometry from the 2 and 3 pixel apertures showed excellent agreement (dispersion of  $\approx 0.02$ -0.05 magnitudes) through  $\sim 13.5$ -14th (15th) magnitude for the [5.8] and [8] ([3.6] and [4.5]) channels. Beyond these limits, the dispersion in magnitudes increased to  $\sim 0.15$  mag. The measured pixel area of  $\gtrsim 13$ th magnitude stars is completely enclosed by the 2-pixel aperture radius. Therefore, we chose photometry from the 2-pixel aperture for stars fainter than 13th magnitude in all filters and the 3-pixel aperture for brighter stars. Catalogs were constructed for both the 0.6s and 10.4s exposures and trimmed of sources lying within 5 pixels of the mosaic edges.

To check the photometry, we compared aperture magnitudes with results from SExtractor. The differences between SExtractor and IDLPHOT magnitudes are typically small,  $\lesssim 0.025$  mags, through 13th-14th magnitude in all filters. For the long IRAC exposures, stars brighter than  $\sim 7$ th-9th magnitude are saturated in all bands, with negative pixel counts in

---

<sup>2</sup><http://ssc.spitzer.caltech.edu/irac/dh/iracdatahandbook3.0.pdf>

the centers of the brightest stars. Therefore, we identified stars with  $m[\text{IRAC}] \leq 9$  in any band from the 0.6s catalog and replaced their counterparts in the 10.4s catalog. To merge the final IRAC catalog with the 2MASS JHK<sub>s</sub> catalog, we employed a 2'' matching radius between 2MASS and IRAC, resulting in 16204, 16477, 9417, and 6087 matches in the [3.6], [4.5], [5.8], and [8] channels.

The photometric errors are calculated from the Poisson error in the source counts, the read noise, the Poisson error in the background level, and the uncertainty in the background ( $\sigma_{\text{bgd},\text{rms}}$ ). Figure 1 (top panel) shows that the source counts in the IRAC bands peak at [3.6]  $\sim 16$ , [4.5]  $\sim 16$ , [5.8]  $\sim 15$ , and [8]  $\sim 14.25$ -14.5. The IRAC photometry approaches the  $10\sigma$  limit at [3.6]  $\sim 16.5$  (70.56  $\mu\text{Jy}$ ), [4.5]  $\sim 16.5$  (45.13  $\mu\text{Jy}$ ), [5.8]  $\sim 14.25$  (229.46  $\mu\text{Jy}$ ), and [8]  $\sim 14$  (161.09  $\mu\text{Jy}$ ).

Because the MIPS point-spread function is well characterized, we performed photometry on the 24 $\mu\text{m}$  and 70 $\mu\text{m}$  MIPS data with pixel response function (PRF) fitting with APEX. We detect 2,702 sources at [24] and 438 sources at [70]. To identify candidate stellar sources, we merged the MIPS catalogs with 2MASS using matching radii comparable to the median position errors in MIPS: 2'' for the 24  $\mu\text{m}$  channel and 4'' for 70  $\mu\text{m}$ <sup>3</sup>. There are 526 MIPS 24 $\mu\text{m}$  sources with 2MASS counterparts and 66 70 $\mu\text{m}$  sources with 2MASS counterparts. The bottom panel of Figure 1 shows the distribution of the 24  $\mu\text{m}$  and 70  $\mu\text{m}$  MIPS magnitudes for these sources. The source counts peak at [24]  $\sim 10.5$  ( $\sim 460$   $\mu\text{Jy}$ ) and [70] ( $\sim 20$  mJy). The corresponding peak in the 2MASS J filter for sources detected at [24] is  $J \sim 11$ . The (5)  $10\sigma$  limits are [24]  $\sim (10.5) 9.75$  and [70]  $\sim (4) 3.5$ <sup>4</sup>. Within the IRAC coverage, most MIPS 24  $\mu\text{m}$  detections with 2MASS counterparts are brighter than  $J=11$  but the 70 $\mu\text{m}$  data yield no 2MASS matches brighter than  $J=14.5$ . Most of the 70  $\mu\text{m}$  sources are faint in 2MASS ( $J \sim 16$ ), have very red near-IR colors, and are probably extragalactic sources. Therefore, we restrict our analysis to the IRAC and MIPS 24  $\mu\text{m}$  bands. Table 1 lists the full photometric catalog for sources detected in at least one IRAC channel or the MIPS 24  $\mu\text{m}$  band.

Many of the MIPS sources without 2MASS magnitudes are galaxies or highly-reddened background stars. Using the number density of galaxies in the 24  $\mu\text{m}$  filter from Papovich et al. (2004), we expect  $\sim 1400$ -1700 extragalactic sources in 1.4 square degrees. Typical fluctuations in the galaxy counts are  $\sim 50\%$  (Papovich et al. 2004); thus all of the unmatched MIPS sources could be galaxies. Alternatively, highly-reddened background MIPS sources

---

<sup>3</sup>Setting the matching radii to the median position errors guards against false detections with the risk of not identifying true MIPS counterparts whose positional offsets are greater than 2''.

<sup>4</sup>The uncertainties quoted here do not include the zero-point uncertainty, which is  $\approx 4\%$ .

with 2MASS JHK<sub>s</sub> fainter than the  $10\sigma$  completion limit may lack near-IR detections. This region of the sky contains clusters with regions of high column density interstellar gas (e.g. Orion Nebula Cluster), which may have a very large distributed population as well as background embedded clusters (e.g. Rosette Nebula). Some sources may also have positions determined from the MIPS mosaic that lie  $> 2''$  away from their 2MASS positions.

## 2.2. ROSAT X-Ray Observations of NGC 2232

To supplement the Spitzer data, we queried the High Energy Astrophysics Science Archive Research Center database (HEASAR; NASA-Goddard Space Flight Center<sup>5</sup>) for ROSAT detections from the High-Resolution Imager (HRI) within 2 degrees of NGC 2232. Our x-ray source list is drawn from the ROSHRITOTAL, Bright and Faint Source, and Brera Multi-scale Wavelet catalogs (Voges et al. 1999; Panzera et al. 2003). Observations consist of two separate pointings which cover most of the Spitzer field. Exposures were taken in 20ks, 48ks or 30ks, 36ks pairs. Two additional bright x-ray sources were observed with 0.148 ks integrations. The HRI instrument has a resolution of  $\sim 5''$  in the center of the field.

The ROSHRITOTAL catalog lists all sources detected by the Standard Analysis Software System in processed public HRI datasets. This catalog lists 299 detections, many of which are multiple detections of the same source. The Brera catalog consists of sources identified from a wavelet detection algorithm, which accurately identifies point sources and extended sources (Panzera et al. 2003). The Brera catalog contains 68 sources within the NGC 2232 field detected at a signal-to-noise (SNR)  $> 4.2$ . The faint and bright source catalogs add 35 and 5 detections.

To find 2MASS sources with x-ray counterparts, we combined the ROSAT and 2MASS/Spitzer catalogs using a  $5''$  matching radius comparable to the ROSAT positional accuracy. Merging the catalogs yields 79 2MASS sources with x-ray counterparts. The distribution of positional offsets between 2MASS and ROSAT coordinates show that most fall within  $\sim 2''$ - $3''$  of the 2MASS positions. In one case, a single ROSAT source falls within  $5''$  of multiple 2MASS sources. We chose the source with the smaller positional offset ( $2.8''$  vs.  $3.2''$ ). The source  $3.2''$  from the ROSAT coordinate also has 2MASS colors indicating it is a background early-type star.

---

<sup>5</sup><http://heasarc.gsfc.nasa.gov/W3Browse/>

### 2.3. Optical Photometry from Claria (1972) and Lyra et al. (2006)

We also include optical UBV and BVI photometry from Claria (1972) and Lyra et al. (2006). These data 1) identify a cluster sequence for bright stars and 2) provide a longer wavelength baseline. The Claria (1972) photometry catalog was downloaded from the WEBDA open cluster database. The catalog contains  $\sim 43$  sources with  $V \lesssim 12$ . Initial positions in B1950 coordinates were inspected for accuracy. Fortunately, all stars are bright enough to have HD numbers and precise positions from the Hipparcos and Tycho catalogs. Based on these measurements, we adjusted the coordinates from Claria (1972) and precessed them into J2000 coordinates.

The Lyra et al. (2006) survey focused on a much smaller area ( $\sim 15' \times 15'$  centered on the cluster) but went deeper (to  $V \sim 20$ ). The survey identified 1,407 stars within this region. We merged the Claria (1972) and Lyra et al. (2006) catalogs with the 2MASS and Spitzer catalogs, using a  $2''$  matching radius.

Claria (1972) used multiple optical color-magnitude and color-color diagrams to identify stars defining a locus consistent with a cluster, to derive the interstellar reddening to each star, and to estimate the age of the cluster. From these methods, Claria (1972) identifies at least 19 early-type stars consistent with cluster membership, computes a mean reddening of  $E(B - V) \sim 0.01$ , and estimates a nuclear age of  $\sim 20$  Myr. Lyra et al. (2006) show that by ‘subtracting’ (in  $V/V-I$  space) a field population from that containing the cluster, potential cluster members remain which define a clear *empirical* isochrone for the cluster. They compute an age of  $\sim 25$ -30 Myr and a slightly larger typical reddening of  $E(B-V) \sim 0.07$ . Our motivation for including these data is to compare the colors of candidate cluster members in the ROSAT and Spitzer samples with known cluster members from Claria (1972) and the locus of cluster members from Lyra et al. (2006).

### 2.4. Optical Spectra

To explore the NGC 2232 stellar population in more detail, we downloaded spectra of stars in the NGC 2232 field from the FAST data archive housed at the Telescope Data Center at the Smithsonian Astrophysical Observatory. Spectra were taken by the FAST instrument on the 1.5m Tillinghast telescope on January 31, 2001 as a part of the FAST combo queue observing program (PI: Brian Patten). We also took FAST spectra of ID 18012 on April 14, 2008 (PI: Thayne Currie). The data were taken with the  $270 \text{ g mm}^{-1}$  grating, yielding a wavelength coverage of 4000-9000 Å with 3 Å resolution (Fabricant et al. 1998). We identify 38 separate sources in the 2001 data archive, 36 of which have high enough signal-to-noise

to analyze.

To derive quantitative spectral types, we first compared equivalent widths of the H I Balmer lines, CaII H and K, G band, Na 5890, and TiO bands with spectroscopic standards from Jacoby et al. (1984). In a second iteration, we computed the spectral types from the semi-automatic spectral typing code SPTCLASS (Hernandez et al. 2004) and from manually measuring the equivalent width of indices with high correlation coefficients from smoothed spectra. Spectral types derived manually and with SPTCLASS agree within 0.5-1 subclasses. Table 2 lists the spectral types of these stars. Many stars originally observed by Claria (1972) were reobserved here. Agreement between spectral types derived here and those from the literature are good to within  $\sim 2$ -3 subclasses.

We show two spectra in Figure 2. Both have red  $K_s$ -[8] colors but very different spectral types. The top panel shows ID 18566, listed as a B9.5 star in Levato and Malaroda (1974) and classified as A2.8 here. The individual indices used to derive the spectral type (e.g. CaII) yield estimates ranging between A0 and A3. Spectral types estimated from the Balmer lines yield A2-A3. ID 18622, shown in the bottom panel, is a Li-poor M3.4 star with  $H_\alpha$  emission ( $EW(H_\alpha) \sim 8 \text{ \AA}$ ). Because this source has a ROSAT detection and the line is single-peaked and rather narrow ( $FWHM < 6 \text{ km s}^{-1}$ ), the emission is likely due to chromospheric activity. Several other stars, all with ROSAT detections, show similar levels of  $H_\alpha$  emission. Thus, we find no strong evidence for a population of late-type stars with strong  $H_\alpha$  emission indicative of accretion ( $EW(H_\alpha) \gtrsim 10 \text{ \AA}$ ; White and Basri 2003).

## 2.5. IRAC and MIPS Colors of Sources with 2MASS counterparts

To make a first assessment of a possible disk population among the Spitzer sources, we consider several color-color and color-magnitude diagrams constructed from 2MASS, IRAC, and MIPS data. Our goal is to isolate stars with excess IR emission from stars with photospheric colors. For the derived age ( $\sim 25 \text{ Myr}$ ), distance (320–360 pc), and reddening ( $A_V \lesssim 0.2 \text{ mag}$ ), early to mid-M type stars in NGC 2232 have  $J \sim 14$ –14.5 and intrinsic 2MASS/IRAC/MIPS colors  $\leq 0.5$ . For the derived sensitivities of the IRAC data, we expect all cluster stars to lie above the  $10\sigma$  limits for all IRAC bands. Thus, we focus our analysis on sources with 2MASS  $J \leq 14.5$ .

NGC 2232 is a sparse cluster (Claria 1972; Lyra et al. 2006). For a normal mass function, the observed population of massive cluster stars implies a total cluster population of  $\sim 500$  stars. Because stars with IRAC excess are rare in young clusters with ages  $\sim 10$ –30 Myr ( $\lesssim 5$ –10%; Currie et al. 2007a; Gorlova et al. 2007), we expect  $\lesssim 25$ –50 stars with IR excess.

There are  $\sim 18,000$  2MASS sources with IRAC counterparts in this region. Compared to massive clusters in relatively low background regions (e.g.  $\eta$  and  $\chi$  Per; Currie et al. 2007a), identifying an obvious main sequence for cluster stars is challenging. Therefore, we concentrate on color-color and color-magnitude diagrams that allow us to isolate (i) background/cluster stars with a well-defined dispersion around the sequence expected for stellar photospheres and (ii) a handful of stars with IR excesses at least  $3\sigma$  larger than the measured dispersion in photospheric colors.

Figure 3 shows the J vs.  $K_s-[8]$  color-magnitude diagram and  $K_s-[5.8]$  vs.  $K_s-[8]$  color-color diagram (top left and top-right panels, respectively). The main distribution of  $K_s-[8]$  colors defines a locus that widens from 0.1 mag at  $J=6$  to  $\sim 0.4$  mag at  $J=14.5$ . The flaring of this locus to  $\sim 0.4$  mag near the faint limit results from a combination of a) larger photometric errors, b) a much wider range of intrinsic colors for both cluster and background stars, and c) a wider range of reddening for background stars. Several sources have  $K_s-[8]$  colors far redder than the main distribution. There are no stars with similarly blue  $K_s-[8]$  colors. The main distribution of  $K_s-[5.8]/K_s-[8]$  colors extends from  $K_s-[5.8] = -0.1$  to 0.2 and  $K_s-[8] = -0.2$  to 0.3 (Figure 3, top-right panel). Few sources with very red  $K_s-[5.8]$  colors have blue  $K_s-[8]$  colors. Most sources with red  $K_s-[5.8]$  colors also have red  $K_s-[8]$  colors. The sources with very red  $K_s-[8]$  colors could plausibly be cluster members with warm circumstellar dust.

Many sources in Figure 3 (bottom-left panel) have  $K_s-[24]$  colors greater than  $\sim 0.5$  and as large as 5. These excess sources lie in two groups. The first group has  $J \sim 6-10$  with  $K_s-[24] \sim 0.5$  to 2.25. If these stars are 25 Myr-old cluster members, they are massive stars with B0–F5 spectral types. The second group has  $J \sim 12-14$  with  $K_s-[24] \sim 2-5$ . If these sources are cluster members, they are low-mass stars with K5–M6 spectral types.

In addition to stars with IR excess, the NGC 2232 field has a clear sequence of stars with colors of normal main sequence stars (Figure 3, bottom left panel). This sequence begins at  $J, K_s-[24] \sim 5, 0$  and extends to  $J, K_s \sim 10, -0.25$  to 0.25. At  $J \sim 10-11$ , the sequence broadens considerably and then develops a red tail of sources with very red  $K_s-[24]$  colors. With measured  $5-10\sigma$  sensitivity limits of 9.75–10.5 (§2.1), the MIPS images cannot detect stellar photospheres with  $J \gtrsim 11$ . Thus, many K and M stars detected by MIPS are probably  $24 \mu m$  excess sources.

Figure 3 (bottom-right panel) shows that many of the stars with photospheric  $K_s-[8]$  colors have excess emission at  $24 \mu m$ . The main distribution of colors ranges from  $K_s-[8] \sim -0.1$  to 0.1 and  $K_s-[24] \sim -0.2$  to 0.3. We find no evidence for sources with red  $K_s-[8]$  colors but blue  $K_s-[24]$  colors. About six sources have  $K_s-[8] \gtrsim 0.3$  and  $K_s-[24] \gtrsim 1$ . These stars have substantial warm circumstellar dust, have intrinsically red photospheres (see §4.1), or

are heavily reddened.

Figure 3 demonstrates that some stars in the direction of NGC 2232 have robust detections of IR excess emission. The number of IR excess stars,  $\sim 10$ –20, is comparable to our predicted number of  $\sim 25$ –50. Thus, some of these excess stars are plausibly associated with the cluster. To identify *bone fide* cluster stars and candidate cluster stars among this group, we consider several methods using ROSAT detections, color-magnitude diagrams, and proper motions. Once we have a catalog of confirmed/candidate members, we analyze the disk population in §4.

### 3. Identifying Cluster Members

We now use ROSAT x-ray detections, optical/IR colors, and proper motion to identify candidate cluster members. The positions of ROSAT sources on optical/IR color-magnitude diagrams follow a locus consistent with previously identified cluster members from Claria (1972) and Lyra et al. (2006). This locus allows us to identify additional candidate members from optical/IR color-magnitude diagrams and from proper motion data.

#### 3.1. Catalog of Cluster Members based on X-Ray Active Stars and Claria (1972)

To isolate cluster members from background stars, we first consider the ROSAT detections. Young late-type stars are X-ray active (e.g. Preibisch and Feigelson 2005). For stars with ages  $\sim 10$ –15 Myr, the typical X-ray flux is  $\sim 100$ –1000 times larger than fluxes for stars of similar mass with ages  $\gtrsim 100$  Myr (Chandra Observations of Orion, the Pleiades, and  $\eta$  Persei; Preibisch and Feigelson 2005; Stauffer et al. 2005; Currie et al. 2008c).

Figure 4 shows the ROSAT detections and the Claria (1972) cluster members on a J/J-Ks color-magnitude diagram. These stars define a clear locus consistent with the isochrone expected for a 25 Myr-old cluster. Bright cluster members from Claria (1972) trace the isochrone well for  $J = 6$ –10. For  $J \geq 10$ , the ROSAT detections clearly indicate the location of the cluster, isolating it from brighter (fainter) foreground red dwarfs (background red giants) with  $J \lesssim 10$  and  $J-K_s \gtrsim 0.6$  and the large background population with  $J \gtrsim 12$  and  $J-K_s \sim 0$ –0.6.

ROSAT sources outside the 25 Myr isochrone are mostly faint background stars. Stars with  $J = 14$ –14.5 and  $J-K_s = 0.4$ –0.8 have bluer  $J-K_s$  colors than cluster stars at the same  $J$ . The apparent magnitudes of these stars are consistent with young stars at distances  $\sim$

500–1000 pc and thus might be members of more distant clusters or star-forming regions.

### 3.2. Candidate Members Identified from Lyra et al. (2006) and 2MASS photometry

The ROSAT detections suggest that we can use optical or optical/IR color-magnitude diagrams to identify candidate members. To test this possibility, we compare the V/V-J colors for cluster members identified by ROSAT and Claria (1972) with other stars in the field. We use V-band photometry from Lyra et al. (2006) and photometry from Claria (1972) for sources outside Lyra’s coverage.

Figure 5 shows that the ROSAT and Claria stars define a tight locus in V/V-J space. From these stars, we define an empirical isochrone for the cluster (solid line) with an upper limit to include binaries and a lower limit to allow for slight differences in reddening/distance/age. This empirical isochrone is identical to the Siess et al. (2000) theoretical isochrone for 25 Myr-old  $\gtrsim 0.5 M_{\odot}$  (M0-M1) stars, brighter (bluer) than  $V \sim 16$  ( $V-J \sim 3.2$ ). To match the empirical locus of x-ray active stars<sup>6</sup>, we shift the isochrone redward by  $\sim 0.5$  magnitudes for  $V \geq 16$ .

Compared to Figure 4, Figure 5 has many fewer bright red stars lying above the isochrone, which are likely foreground late-type stars or background giants. This difference probably results from the smaller spatial coverage of Lyra et al. (2006), who focus on the cluster center. To test this possibility, we compare the relative areas of the Lyra et al. (2006) and the IRAC/MIPS surveys. The IRACS/MIPS coverage is  $\sim 22.5$  times that of the Lyra et al. (2006) data. Thus, we expect 22.5 times as many bright, red stars in Figure 4 as in Figure 5. The observed ratio of  $\sim 125/4 \approx 31$  is reasonably close to our expectation.

Because cluster members define a narrow locus in V/V-J space, we identify candidate cluster members lying along this locus between the upper and lower bounds (+0.5, -0.75 mags; dotted lines) in Figure 5. We also identify stars outside the Lyra et al. (2006) coverage but overlapping the area enclosed by confirmed members with positions on the J/J-H and J/J- $K_s$  color-magnitude diagrams consistent with cluster membership (Figure 6). Candidate members are drawn from a more narrowly defined locus ( $\pm 0.5$  mags). We make additional passes through J/J- $K_s$  and J/J-H color space and reject all candidate members that clearly lie outside the plausible color-magnitude range in either diagram.

---

<sup>6</sup>This shift allows us to match the luminosity and colors of stars with masses  $\lesssim 0.5\text{--}0.6 M_{\odot}$  and to account for uncertainties in low-temperature opacities that affect stellar atmosphere models (Baraffe et al. 1998).

### 3.3. Additional Selection Criteria and the Final Membership List

To provide a final check on our membership catalog, we compare the proper motions of previously identified members and other stars on the field. The median proper motion of the cluster is derived from Tycho observations of the early-type members in the Claria (1972) catalog. These stars have a mean proper motion of  $\Delta_{ra,dec} \sim -5.33 \pm 1.27, -2.68 \pm 1.34$  mas yr<sup>-1</sup>. We identify all stars within  $2\sigma$  (of their measurement errors) as having a proper motion consistent with cluster membership. All members in the Claria (1972) catalog meet this criteria. Using the Tycho catalog, Guide Star Catalog, and Henry Draper catalog, we identify field stars and potential cluster members. We reject three bright stars (IDs 2162, 15449, and 18442) and add two stars (IDs 5494 and 5625) whose proper motions are within  $1\sigma$  of the mean cluster motion. We also add one source from our spectroscopic catalog, ID 10258, which has J/J-K<sub>s</sub> and J/J-H positions barely outside our photometric membership criteria. This star has a J magnitude and colors very similar to other K5-M0 cluster members.

In total, we identify 11 members from the Claria (1972) catalog, 37 members from x-ray activity, and two members from proper motion. To this sample we add, 15 candidate members from V/V-J colors and 176 candidate members from J/J-K<sub>s</sub> and J/J-H diagrams, bringing the total to 239 confirmed/candidate members. Of these candidates, 209 have IRAC and/or MIPS photometry. Thus, the cleaned list of x-ray active and previously identified members are photometrically (in two color-magnitude diagrams) and, in some cases, astrometrically confirmed as members. The list of candidate members are all photometrically consistent with membership. Of confirmed/candidate cluster members, 32 have optical spectra listed in Table 2. Table 3 lists all the confirmed/candidate members with Spitzer photometry.

The candidate members identified from color-magnitude diagrams contain a potentially large population of field stars, especially for stars with near-IR colors consistent with foreground M stars and background M giants (J-H  $\sim 0.6$ - $0.7$ , J-K<sub>s</sub>  $\sim 0.75$ - $0.85$ ). To better constrain their status, these sources need additional photometric and spectroscopic data. In the analysis section, we retain these sources with the qualifier that some are probably not cluster members. Thus, though candidate members identified from optical and near-IR color-magnitude diagrams may include NGC 2232 sources with IR excess, including all candidate members identified from these diagrams necessarily introduces uncertainties in determining the frequency of disks for stars later than  $\sim$  F0-G0. The samples of confirmed and candidate cluster members are, in order from most to least robust, the x-ray active sources and the Claria (1972) catalog, sources selected based on V/V-J and proper motion, and sources selected based on J/J-K<sub>s</sub>.

## 4. Analysis of the NGC 2232 Disk Population

### 4.1. IRAC/MIPS colors of Cluster Members

We now analyze the IRAC and MIPS colors of confirmed and candidate NGC 2232 members. Figures 7 and 8 show the  $K_s$ -[4.5], [5.8], [8], and [24] colors for these stars. Overplotted are the loci for photospheric colors of (pre) main sequence stars (vertical dashed line) and the giant locus (vertical dot dashed line); J- $K_s$  colors for A0-M5 stars are identified by horizontal dotted lines. The loci for photospheric colors were derived from the STAR-PET interactive tool on the *Spitzer Science Center* website, which computes 2MASS-Spitzer colors based on the Kurucz-Lejeune stellar atmosphere models (e.g Kurucz 1993; Lejeune et al. 1997) convolved with the IRAC and MIPS filter responses (Table 4). We also overplot the reddening vector assuming the 2MASS/IRAC reddening laws from Indebetouw et al. (2005);  $A_{24}$  is estimated from Mathis (1990).

For stars with photospheric near-IR emission and identical extinction, the J- $K_s$  color separates stars by spectral type. Cluster stars follow a well-defined locus in the near-IR/IRAC color-color diagrams (Figure 7). From early to late-type stars, the full dispersion about the photospheric locus ranges from  $\sim 0.05$  to  $0.1$  mag, roughly twice the maximum photometric error at [5.8, 8]. There are no cluster stars with red giant colors ( $J-K_s \gtrsim 0.9$ ) or with the colors of the lowest-mass main sequence stars ( $\gtrsim$  M4 spectral type). The lack of red giant stars suggests our selection criteria are robust. The lack of stars later than M4-M5 is consistent with our J-band magnitude cutoff for IRAC sources with  $10\sigma$  detections.

NGC 2232 contains a small population of stars with  $5.8\mu m$  and/or  $8\mu m$  excesses. One star (ID 18566) with a blue J- $K_s$  color has a  $K_s$ -[4.5, 5.8, 8] excess ( $\sim 0.2, 0.5, 1$  mags) clearly larger than the zero  $K_s$ -[4.5, 5.8, 8] color expected for early-type stellar photospheres. The stellar spectrum confirms the A spectral type suggested by the J- $K_s$  colors and shows no evidence for accretion (Figure 2). Visual inspection of the source on the IRAC and MIPS frames shows no evidence for source blending (Figure 9, left panel).

While most late-type stars in the cluster have photospheric colors, a few may have  $K_s$ -[5.8, 8] colors  $\gtrsim 0.2$ - $0.3$  mag redder than the photosphere. IDs 6540, 9220, 18601, and 18622 have  $8\mu m$  excesses that are  $\geq 3\sigma_{[5.8],[8]}$  away from the right-hand vertical dotted line showing the  $0.1$  magnitude bound for photospheric sources. Thus, these stars have red  $K_s$ -[IRAC] colors that may indicate the presence of warm, circumstellar dust.

One star (ID 6540) with red J- $K_s$  colors appears to have a  $\sim 0.7$  magnitude excess at  $8\mu m$ . ID 6540 may also have a borderline ( $\sim 0.27$  mag) excess at  $5.8\mu m$ . Although the image mosaic at  $5.8\mu m$  does not show contamination from another source, the  $8\mu m$  image

is slightly extended and may be blended. Blending could arise from the superposition of ID 6540 with a background galaxy. Galaxies have much redder  $[5.8]-[8]$  colors than stars; thus a background galaxy can raise the  $8\ \mu\text{m}$  flux of a stellar source and remain undetected at shorter wavelengths. Thus, the excess for this source is questionable.

The other late-type stars with  $8\ \mu\text{m}$  excess are not artificially brightened by source blending (e.g. ID 18601; see Figure 9, right panel). Another source with very red  $K_s-[5.8, 8]$  colors, ID 18622, also lacks evidence for blending. The IRAC mosaics show that these stars have no neighbors whose light partially falls within their aperture radii. These sources are also  $\sim 12\text{th}$ - $13\text{th}$  magnitude, corresponding to an IRAC flux  $\sim 4$ - $15$  times brighter than the  $10\sigma$  limits in these filters. Thus, NGC 2232 may contain a late-type population of stars with warm dust emission. In contrast, all sources with  $J-K_s \sim 0.2$ - $0.7$  (plausibly F0-K5 stars) have photospheric colors.

The population of potential  $24\ \mu\text{m}$  excess sources is larger (Figure 8). Many cluster stars with blue  $J-K_s$  colors have  $24\ \mu\text{m}$  fluxes up to  $\approx 3$ - $10\times$  their predicted photospheric fluxes ( $K_s-[24] \sim 1$ - $2.5$ ). Other members with slightly redder colors ( $J-K_s \sim 0.2$ - $0.5$ ; plausibly F0-K0 stars) may also have weak excess emission ( $\sim 0.25$ - $1$  mags). Figure 8 (left panel) reveals a third population of stars with  $K_s-[24] \sim 0.5$ - $1.5$  that are plausibly K/M stars. While the errors in  $[24]$  are larger at a given magnitude than in the IRAC bands, the excesses are typically much larger than IRAC excesses. In §2 we showed that the number counts of MIPS-detected stars peak at  $[24] \sim 10.5$  and  $J \sim 11$ . Assuming a distance of 340 pc, an extinction of  $E(B-V) = 0.07$ , and a cluster age of 25 Myr, 11th magnitude cluster stars should have a G2 spectral type. Thus, the MIPS survey is likely complete to early G stars. While MIPS does not detect the photospheres of stars later than  $\sim G2$ , it can detect late-type stars with  $24\ \mu\text{m}$  excesses from circumstellar dust.

All but one of the MIPS-excess sources appear to have photospheric IRAC colors (Figure 8, top-right panel). The confirmed, early and intermediate-type (B-G) NGC 2232 members have a range of  $24\ \mu\text{m}$  excesses ranging from  $\sim 0.3$  to  $2.2$  mag. However, all but one have a very narrow range of  $K_s-[8]$  colors ( $\sim -0.1$  to  $0.1$ ) consistent with stellar photospheres. The later-type sources with  $\sim 0.3$ - $0.9$  mag  $24\ \mu\text{m}$  excesses from Figure 8 (top-left panel and bottom-left panel) also have a narrow range of  $K_s-[8]$  colors ( $\sim 0$ - $0.15$ ) consistent with late-type photospheres. Sources lacking  $8\ \mu\text{m}$  excess also have a range of  $K_s-[5.8]$  and  $K_s-[4.5]$  colors consistent with photospheres.

## 4.2. SED Modeling of HD 45435 (ID 18566): Evidence for Debris Emission Produced From Terrestrial Planet Formation

NGC 2232 has many good candidates for debris disks. In addition to a handful of stars with modest IRAC excesses, there are many cluster members with  $24\ \mu\text{m}$  excess emission. The level of this excess emission ( $\sim 0.5\text{--}2.25$  mags) is much smaller than excesses in primordial disks ( $\sim 5$  mags; Kenyon and Hartmann 1995; Hernandez et al. 2007; Currie and Kenyon 2008); however, the levels are similar to the excesses observed in debris disks ( $\sim 0.5\text{--}3$  mags; Rieke et al. 2005; Su et al. 2006; Gorlova et al. 2007; Currie et al. 2008a).

To test whether the excess sources are primordial disks, evolved primordial/transition disks, or debris disks, we rely on analyses of spectral energy distributions (SEDs) and the ratio of the observed fluxes to predicted photospheric fluxes at  $8\ \mu\text{m}$  and at  $24\ \mu\text{m}$ . Only one star, ID 18566 with an A3 spectral type, has clear excesses in the IRAC and MIPS bands. These excesses allow us to measure the temperature and luminosity of the dust. As shown below, our analysis demonstrates that this star harbors a debris disk. Other sources with IRAC (MIPS) excesses have no obvious MIPS (IRAC) excesses. Thus, we cannot analyze the SED in detail. Because the excesses for these sources are smaller than those for ID 18566, these stars probably also harbor debris disks. In §4.3, we show that the observed excesses and upper limits at other wavelengths are consistent with this conclusion.

To analyze the SED for HD 45435, we follow the procedure from Augereau et al. (1999) and Currie et al. (2007b, 2008a). The star+disk emission is first fit to a sum of the stellar blackbody plus two scaled blackbodies from the disk to derive a) the amount of disk emission relative to the star and b) the temperature, and thus location, of the disk emission. We assume uncertainties of 5% (10%) in the IRAC (MIPS) bands due to possible systematic effects (e.g. uncertainty in the zero-point flux, phase-dependent response, and photometric errors). Evolved primordial disks such as transition disks in IC 348 and Taurus have fractional luminosities,  $L_d/L_\star \approx 0.1$  (Calvet et al. 2005; Low et al. 2005; Currie and Kenyon 2008). Debris disks have disk luminosities  $\gtrsim 100$  times smaller than evolved primordial disks ( $\approx 10^{-5}\text{--}10^{-3}$ , e.g. Padgett et al. 2006; Su et al. 2006; Rhee et al. 2007a; Currie and Kenyon 2008). Thus, the disk luminosity discriminates between disks of different evolutionary states.

Second, the source SED is compared to more rigorous disk models. We consider an evolved primordial disk model from Kenyon and Hartmann (1987), a terrestrial zone debris disk model from Kenyon and Bromley (2004), and a cold debris disk model from Kenyon and Bromley (2008). For the evolved primordial disk model, the disk temperature scales as  $T \propto r^{-3/4}$ . We vary the inner hole size to match the level of IRAC emission. Debris from terrestrial planet formation is modeled at 1.5–7.5 AU from a  $2.0\ M_\odot$  star

(Kenyon and Bromley 2004). For the cold debris disk model, debris from planet formation is modeled at 30–150 AU from a  $2.0 M_{\odot}$  star (Kenyon and Bromley 2008).

The  $\min(\chi^2)$  scaled blackbody fit for HD 45435 shown in Figure 10 demonstrates that the amplitude of disk emission ( $L_d/L_{\star} \sim 5 \times 10^{-3}$ ) is comparable to the most luminous debris disks (e.g. HD 113766A and  $\chi$  Per-S5, see Lisse et al. 2008; Currie et al. 2008a) that the disk has very hot dust. The fits require dust populations at two different temperatures,  $\sim 360$  K and 815 K. This emission is consistent with warm dust in regions comparable to the orbits of Mercury and Earth in the Solar System. Disk emission clearly emerges above the stellar photosphere by  $3.6 \mu m$  and dominates over the photosphere longwards of  $8 \mu m$ .

Comparing the source SED to predictions from transition and debris disk models confirms that the HD 45435 likely harbors a terrestrial zone debris disk. The transition disk model drastically overpredicts the mid-IR flux longwards of  $\sim 4\text{--}5 \mu m$ . The cold debris disk fares better in reproducing the MIPS excess. However, it predicts only marginal  $5.8 \mu m$  and  $8 \mu m$  excesses in contrast to the strong excesses observed. The terrestrial zone debris disk models accurately reproduces the IRAC and MIPS fluxes.

In summary, HD 45435 (ID 18566) has the strongest  $24 \mu m$  excess of any NGC 2232 member and is the only source with a strong IRAC excess. Compared to other cluster members, its disk is the most likely to be at an early evolutionary state, perhaps an evolved primordial disk/transition disk. However, SED modeling suggests that this source is instead a warm debris disk. The SEDs of sources with weaker  $24 \mu m$  emission are even more optically thin and more likely to be debris disks. Thus, optical spectroscopy and SED modeling suggest that the mid-IR excesses from early-type stars in NGC 2232 are due to dust in circumstellar debris disks.

### 4.3. Frequency of $8 \mu m$ and $24 \mu m$ Emission from Debris Disks

We now consider the frequency and nature of the stars with excess IRAC (MIPS) emission but no statistically significant MIPS (IRAC) excess. After defining robust criteria for these sources, we measure the frequency of disk emission in both bands. To place initial constraints on the disk properties of these sources, we use IRAC and MIPS upper limits to constrain the dust temperature and to derive a lower limit to the dust luminosity. These results demonstrate that NGC 2232 members include at least two stars with warm debris disks and many stars with cold debris disks.

#### 4.3.1. Frequency of 8 $\mu m$ Emission

With the exception of HD 45435, NGC 2232 lacks any stars with very luminous 8  $\mu m$  excess emission (e.g. greater than twice the photospheric flux). Warm dust around other stars must be far weaker. The preceding section (§4.1) identifies several stars with  $K_s$ -[8] colors redder than  $3\sigma$  away from theoretical photospheric colors. However, more robust measures for establishing excess sources are needed. Specifically, the Kurucz-Lejeune synthetic  $K_s$ -[8] colors used to determine photospheric colors (and thus excess sources) are prone to systematic uncertainties in the model atmospheres. Young M stars, which comprise the majority of the 8  $\mu m$  excess candidates, are chromospherically active and can have large fractions of their surfaces covered with starspots, causing changes in the brightness of colors of  $\sim 0.1$  magnitudes (Bouvier et al. 1993). Thus, sources with near IR and mid-IR data taken at different epochs may have an intrinsically larger dispersion in colors at a given spectral type. This dispersion results in a larger uncertainty in measuring the amount of IR excess emission. Because NGC 2232 was not observed in  $K_s$  and [8] simultaneously, starspots may also contribute small uncertainties in identifying excess sources based on the  $K_s$ -[8] color.

To minimize the impact of systematic errors in identifying stars with 8  $\mu m$  excess emission, we determine the locus of photospheric colors empirically from IRAC fluxes. Following Carpenter et al. (2006), we use the [4.5] filter to define the stellar photosphere and compare its flux to the 8  $\mu m$  flux to identify excess sources:  $\log(F[8]/F[4.5])$ . Using the 4.5  $\mu m$  flux has several advantages over using  $K_s$ . The scatter in the [4.5]-[8] color as a function of [8] for all IRAC-detected stars (not shown) is slightly smaller than that in  $K_s$ -[8]. All sources with 8  $\mu m$  detections should also have detections at 4.5  $\mu m$ . Furthermore, the theoretical  $K_s$ -[8] colors from the Kurucz-Lejeune stellar atmosphere models suggest that the [8] to  $K_s$  flux ratios as a function of spectral type cannot be fit by a linear function, whereas the [8] to [4.5] flux ratios can (Carpenter et al. 2006). Finally, the 8  $\mu m$  to 4.5  $\mu m$  flux ratio is insensitive to variations in reddening because stars are reddened by the same amount in either filter (Indebetouw et al. 2005).

Using  $4\sigma$  iterative clipping, we calculate a best-fit line using a standard linear least-squares fit to the locus of cluster stars in  $J$ - $K_s$  vs.  $\log(F[8]/F[4.5])$  space. The final linear fit has a slope of 0.046 and a y-intercept of -0.465 with rms residuals of  $\sim 3.92\%$ . To determine an empirical excess criterion, we identify the threshold, in  $\sigma_{rms}$ , beyond which there are no sources with 'negative excesses' (deficient flux ratios):  $\sim 3.42\sigma_{rms}$ . Assuming a dispersion in IRAC colors dominated by photon noise, we expect less than 1 star out of 200 cluster members detected at 8  $\mu m$  to be more than  $3-4\sigma_{rms}$  away from the photospheric locus. We adopt a  $4\sigma_{rms}$  threshold to identify cluster stars with 8  $\mu m$  excesses. Similar thresholds have been adopted by other authors to identify stars with weak excesses in both IRAC and MIPS

(e.g. Carpenter et al. 2006; Hillenbrand et al. 2008).

NGC 2232 includes four stars that are  $\geq 4\sigma_{rms}$  away from the photospheric locus in  $\log(F[8]/F[4.5])$  (Figure 11). For confirmation of these excesses, we compare their  $K_s-[8]$  colors to photospheric predictions. ID 18613, a cluster member identified by x-ray activity, has a  $4.35\sigma$  excess in the  $8\mu m$  to  $4.5\mu m$  flux ratio but has a rather blue  $K_s-[8]$  color ( $\sim 0.183$ ) consistent with photospheric predictions. However, three stars – IDs 6540, 9220, and 18566 – have flux ratio excesses and red  $K_s-[8]$  colors lying outside the locus of predicted photospheric colors. The apparent excesses for these stars are more than  $3\sigma$  larger than their photometric errors. Even though ID 6540 has a  $> 8\sigma$  excess, the previous section cites source blending as a possible source for its excess emission. In contrast, ID 18566 (HD 45435) is not blended and clearly has excess emission from  $4.5\mu m$  onwards. ID 9220 also shows no evidence for blending and has red  $K_s-[8]$  and  $K_s-[5.8]$  colors suggestive of mid-IR excess in addition to its excess in  $\log(F[8]/F[4.5])$ . ID 6540 is identified as a candidate member based solely on near-IR color-magnitude diagrams; ID 9220 is identified as a member from both optical/near-IR and near-IR color-magnitude diagrams. Therefore, at least early-type star and likely one late-type star (ID 9220) in NGC 2232 have bona fide IRAC excesses indicative of warm dust; two other late-type stars may also have warm dust emission. Properties of the four  $8\mu m$  excess sources are listed in Table 5.

While our method can identify IR-excess sources without some systematic uncertainties, it may conceal some bona fide excess sources with very warm dust ( $T_d \sim 350\text{--}600\text{ K}$ ). Using the  $8\mu m$  to  $4.5\mu m$  flux ratios to define excess sources best identifies warm dust whose flux peaks at  $\lambda \gtrsim 8\mu m$ . In terms of their photometric errors, IDs 18601 and 18622 have both  $K_s-[8]$  and  $K_s-[5.8]$  colors ( $\sim 0.4$  mags) greater than  $3\sigma$  away from the locus of predicted photospheric colors. However, their  $8\mu m$  to  $4.5\mu m$  flux ratios are less than  $3\sigma$  away from the empirically-defined photospheric locus. If these systems have weakly-emitting warm dust that peaks in the IRAC bands, then their  $8\mu m$  to  $4.5\mu m$  flux ratios will be bluer than that for dust whose  $8\mu m$  emission is on the Wien tail of a slightly colder blackbody.

We adopt a simple model to show that the weak  $8\mu m$  excesses around late-type stars yield disk luminosities consistent with debris disks. To estimate the disk luminosity at  $8\mu m$ , we calculate the flux of the  $8\mu m$  excess, assume that the disk emission peaks at  $8\mu m$  and originates from a 360 K blackbody, and assume the stellar luminosity of a 25 Myr-old M0 star from Siess et al. (2000). We derive  $L_d/L_\star \approx 10^{-4}\text{--}10^{-3}$ , consistent with debris disk luminosities. The maximum disk luminosity from a 120 K blackbody consistent with the  $24\mu m$  upper limits is also  $L_d/L_\star \approx 10^{-3}$ .

To estimate the frequency of  $8\mu m$  emission as a function of stellar mass/spectral type, we divide the sample into 'early' (BA), 'intermediate' (FG), and late (KM) stars based on

their J-K<sub>s</sub> colors. The frequency of 8  $\mu$ m emission in these groups is 6.3% (1/16), < 3.8% (0/26), and 0–1.9% (0-3/158). With the exception of the warm debris disk source HD 45435 (ID 18566), no star plausibly earlier than K0 has 8  $\mu$ m excess. At least one and as many as three late-type stars have large 8  $\mu$ m to 4.5  $\mu$ m flux ratios indicative of warm dust. If two stars (IDs 18601 and 18622) with small  $\log(F[8]/F[4.5])$  but red K<sub>s</sub>-[5.8, 8] colors are also classified as excess sources, the frequency of warm dust around late-type stars could be as high as 3.2%. Optical spectra is required to confirm the membership status of late-type candidate cluster members and thus better constrain the frequency of late-type stars with warm dust.

These results suggest that warm dust surrounding NGC 2232 cluster stars is rare. However, the derived frequencies of warm dust for early-type members are based on a small sample, which precludes a robust determination of the excess frequency for 25 Myr-old B and A stars. Lack of deep x-ray data and incomplete optical spectroscopy prevents robust estimates of membership probabilities for intermediate and late-type stars. These data would allow us to separate true cluster members from foreground M dwarfs and background red giants.

#### 4.3.2. Frequency of 24 $\mu$ m Emission

To identify sources with 24  $\mu$ m excess, we consider the sensitivity of the MIPS data and the photospheric colors of likely cluster members. For  $5\sigma$  detections with [24]  $\approx 10.5$ , MIPS cannot detect the photospheres of cluster stars with spectral types later than  $\sim$  G2. For early G stars, the Kurucz-Lejeune stellar atmosphere models predict K<sub>s</sub>-[8]  $\sim -0.020$  and K<sub>s</sub>-[24]  $\sim 0.005$ . Observations of  $\sim 30$  solar-type stars from Rieke et al. (2008) suggest K<sub>s</sub>-[8]  $\sim 0.046$  and K<sub>s</sub>-[24]  $\sim 0.045$ . Uncertainties in absolute calibration are small,  $\sim 1.5\%$  (Rieke et al. 2008). Older calibrations suggest K<sub>s</sub>-L'/M  $\lesssim 0.02$  for solar-type stars (e.g. Kenyon and Hartmann 1995). Thus, we expect small photospheric colors – K<sub>s</sub>-[24]  $\lesssim 0$  – for all cluster stars detected by MIPS.

Small number statistics and different areal coverage prevent developing an empirical locus of photospheric MIPS colors for all spectral types. There are only 38 candidate/confirmed cluster members detected by MIPS compared to 200 detected at 8  $\mu$ m. Therefore, it is difficult to define the empirical locus of photospheric MIPS colors from early to late spectral types. Because the MIPS coverage is slightly larger than the IRAC coverage at 4.5  $\mu$ m, not all MIPS-detected stars have measured 4.5  $\mu$ m fluxes. Therefore, using the [4.5] filter as a photospheric baseline is not ideal.

Because the expected photospheric colors of B to G stars are small and vary little with spectral type, we develop an excess criterion based on the  $K_s$ -[24] color and the MIPS photometric error:

$$(K_s - [24])_{obs} - (K_s - [24])_{phot} \geq 3\sigma_{24}. \quad (1)$$

To account for systematic errors (e.g. uncertainties in the zero-point flux, phase-dependent response errors, and uncertainties in the model atmospheres) and the observed dispersion of colors, we also require that the excess contribute greater than  $\sim 15\%$  of the total flux at  $24 \mu m$ :

$$(K_s - [24])_{obs} - (K_s - [24])_{phot} \gtrsim 0.15. \quad (2)$$

From Figure 8, it is clear that the frequency of  $24 \mu m$  excess emission is much higher than for  $8 \mu m$  excess emission. As previously noted, the poorer sensitivity of MIPS results in completeness-related bias for cluster members later than  $\sim G2$ ; F and G stars are also typically too faint to have proper motion data and robust x-ray detections. In contrast with the A star population, the census of F and G cluster members is likely incomplete. Thus, we identify excess sources for FGK stars but do not attempt to derive a frequency of  $24 \mu m$  excess emission for these stars.

Based on the criteria for excess, 8/15 B and A cluster stars have  $24 \mu m$  emission from circumstellar dust<sup>7</sup>. We identify two additional excess sources (IDs 4144 and 5494) with J- $K_s$  colors suggestive of F0-K0 stars. Other sources with spectral types between F0 and K0 have red  $K_s$ -[24] colors suggestive of IR excess. Because their colors are less than  $3\sigma$  away from the locus of photospheric sources, we do not classify these sources (IDs 11320, 18591, and 18605) as excess sources. Among the later-type stars, we identify ID 18012 an excess source. The spectral types estimated from photometry ( $\sim K7$ -M0) and spectroscopy (M0) are consistent. Thus, ID 18012 is a rare example of a 10–30 Myr-old M star with substantial debris emission. Table 6 lists properties of the early-type members of NGC 2232 and late-type members with  $24 \mu m$  excess.

---

<sup>7</sup>We count ID 18648 as a late A star from its J- $K_s$  colors, though removing this source from the list of B and A stars does not qualitatively change our analysis.

#### 4.4. Evidence for a Correlation between Rotation and Debris Disk Emission for High-Mass Stars: Massive Primordial Disks May Evolve into Massive Debris Disks

Stellar rotation is another property that can impact the frequency and luminosity of disk emission. With studies traditionally focused on near-IR ground-based observations of young clusters with primordial disks, the connection between disk emission and stellar rotation has been controversial. Many authors (Staassun et al. 1999; Rebull et al. 2004; Makidon et al. 2004) fail to find a correlation. Others, most notably Herbst et al. (2002), claim that slower rotators are more likely to have disk emission. Because the level of disk emission compared to the stellar photosphere is larger in the mid infrared than in the near-IR, *Spitzer Space Telescope* observations of young stars provide a more definitive test of the connection between stellar rotation and disk emission.

Recently, Cieza and Baliber (2007) investigated the stellar rotation-disk emission connection in two young clusters, NGC 2264 ( $\sim 2\text{--}3$  Myr) and the Orion Nebula Cluster ( $\sim 1$  Myr). By comparing the rotation periods and Spitzer/IRAC excesses of high-mass cluster stars (see also Rebull et al. 2006; Irwin et al. 2008), they identify a clear increase in the disk fraction with rotational period. Cieza and Baliber interpret this correlation as evidence in favor of the "disk locking" model for rotational evolution of pre-main sequence stars (e.g. Shu et al. 1994; Bouvier et al. 1997), where the star loses angular momentum from magnetic field interactions with the disk. Thus, the more massive disks (presumably identified by their stronger mid-IR emission) are able to spin down the star more substantially.

If massive primordial disks evolve into massive debris disks, then stellar rotation rates should correlate with the level of debris emission. While MIPS data for the  $\beta$  Pic Moving Group hint at a possible connection between the rotation rate and IR excess in debris disks (Rebull et al. 2008), the authors caution that such a correlation is preliminary. The sample is dominated by GKM stars that can drive strong winds from their convective atmospheres, thus affecting stellar rotation. A more conclusive plan is to compare rotation and MIPS excess in B/A star cluster members, which lack convective atmospheres and generally have stronger  $24\ \mu\text{m}$  excesses.

To test this hypothesis, we combine the MIPS data for B/A star cluster members with the rotational velocity study of Levato (1974). The study derives  $v \sin i$  from the He I (4471 Å) and Mg II (4481 Å) lines with an uncertainty of  $\approx 10\text{--}20\%$ . We match all but three of the members studied by Levato. All of these stars are photometrically, spectroscopically, and astrometrically confirmed as members. None have been identified as Be stars, though the rotation rate of one star, with  $v \sin i \sim 400\ \text{km s}^{-1}$ , is close to the breakup velocity for  $2\text{--}2.5\ M_{\odot}$  stars.

Figure 12 shows that rotation and  $24\ \mu\text{m}$  excess appear correlated. Only one star with  $v\sin i \geq 200\ \text{km s}^{-1}$  has a (marginal) excess of  $\sim 0.27$  mag. In contrast, 75% of stars with  $v\sin i \leq 200\ \text{km s}^{-1}$  have  $24\ \mu\text{m}$  excesses. The MIPS excesses of the slower rotators also extend to much larger amplitudes, up to  $\sim 10\times$  photospheric levels, compared to those of the faster rotators ( $\approx 25\%$  of the photospheric levels). The Kolmogorov-Smirnov test yields a probability of  $\sim 1.6\%$  that there is no correlation between rotation and  $24\ \mu\text{m}$  excess ( $d=0.8$ ). Both B stars and early A stars have excesses and photospheric emission. The mean and median spectral types of stars with  $v\sin i \leq (>) 200\ \text{km s}^{-1}$  are B8.7 and A0 (B7.6 and B6.7).

While a larger sample of B and A stars would provide better statistics, these data support the picture that *massive primordial disks evolve into massive debris disks*. However, several caveats about rotational velocities for early-type stars complicate our interpretation of Figure 12. For example, we only know the component of the rotational velocity along our line of sight, so the true rotation rate is not known. While the effects of  $\sin i$  should wash out in very large samples, they may be important for the NGC 2232 sample alone. To better investigate any connection between rotation and debris emission, these data should be combined with data for other similarly-aged A stars to provide a much stronger statistical significance to any correlation.

## 5. The Evolution of Debris Emission from Planet Formation: NGC 2232 in Context

### 5.1. Evolution of $8\ \mu\text{m}$ Emission

The low frequency of  $8\ \mu\text{m}$  emission from disks in NGC 2232 is consistent with recent Spitzer surveys of other young clusters with substantial populations of warm, terrestrial zone debris disks (Table 7). In  $\eta$  and  $\chi$  Persei (13 Myr), the frequency of  $8\ \mu\text{m}$  circumstellar dust emission rises from  $\sim 1.3\text{--}2.2\%$  (14/1023; 42/1878) for B and A stars to  $\gtrsim 6\%$  (34/523; 50/618) for FG stars (Currie et al. 2007a; Currie 2008). Currie et al. (2007a) cite a lower limit of  $\approx 4\%$  for the frequency of  $8\ \mu\text{m}$  emission from intermediate-type stars. This lower limit is still larger than the upper limit for the early-type excess frequency of B and A stars for  $\eta$  and  $\chi$  Per ( $\approx 3.2\%$ ) and much larger than that for B stars alone ( $\lesssim 1\%$ ). Thus, the frequency of  $8\ \mu\text{m}$  emission is spectral-type dependent at a given age and environment.

For other young clusters, small number statistics prevent a clear measure of the variation of excess  $8\ \mu\text{m}$  emission with spectral type. In NGC 2547 (38 Myr), Gorlova et al. (2007) derive excess frequencies of  $<5\%$  (0/19) for B and A stars,  $\sim 1.5\text{--}5\%$  (1–3/62) for F and G

stars, and  $\sim 1\%$  (3/347) for K and M stars. Several stars studied in Gorlova et al. have  $8\ \mu\text{m}$  excesses but were not classified as excess sources because they lacked detectable excesses at  $5.8\ \mu\text{m}$ . This criterion may preclude detection of colder dust where the  $8\ \mu\text{m}$  excess is on the Wien side of the blackbody. Relaxing the requirement of a clear  $5.8\ \mu\text{m}$  excess in NGC 2547 stars yields a larger frequency of warm dust emission, up to  $\sim 2\%$  (8/347) for M-type stars in this cluster. In NGC 2232, our estimates for the frequency of  $8\ \mu\text{m}$  excess –  $\sim 6\%$  (BA),  $< 4\%$  (FG), and  $\sim 0\text{--}1.9\%$  (KM) – are nearly identical to the results for NGC 2547. Within the errors, the low frequency of  $8\ \mu\text{m}$  emission among AB and FG stars in NGC 2232 and NGC 2547 is qualitatively consistent with results for h and  $\chi$  Per.

Combining results for all four clusters, the frequency of warm dust among 10–30 Myr cluster stars at a given age and environment is small. Across all spectral types, the frequency of  $8\ \mu\text{m}$  emission is  $\lesssim 5\text{--}10\%$ . Although NGC 2232 and NGC 2547 have relatively sparse populations of stars with G or earlier spectral types ( $\sim 150$ ), the large population in h and  $\chi$  Per ( $\gtrsim 2000$ ) yields a robust estimate for the frequency of warm dust among early and intermediate-type stars (Currie et al. 2007a). Current data preclude  $8\ \mu\text{m}$  measurements for K and M stars in h and  $\chi$  Per. However, the large populations in NGC 2232 (158) and NGC 2547 (347) demonstrate that warm dust at levels  $L_d/L_\star \gtrsim 10^{-3}$  is rare among 10–30 Myr old K and M stars.

## 5.2. Evolution of $24\ \mu\text{m}$ Emission

Previous Spitzer studies of 5–100 Myr-old clusters examine the time evolution of  $24\ \mu\text{m}$  excess emission around A stars. Using somewhat different samples of nearby A stars, Rieke et al. (2005) and Su et al. (2006) show that the maximum amount of excess emission at a given stellar age declines inversely with age from  $\sim 30\text{--}50$  Myr to  $\sim 1$  Gyr. Currie et al. (2008a) add results for several young clusters to this sample and demonstrate that the maximum level rises for stars with ages of 5–10 Myr, peaks for stars with ages of 10–20 Myr, and then declines inversely with time. With new results for NGC 2232 and NGC 2547, we can reinvestigate ‘the rise and fall of debris disks’ and consider, for the first time, the relative frequency of debris disks for A stars in young clusters.

To investigate the evolution of  $24\ \mu\text{m}$  emission among A stars in young clusters, we consider clusters with good statistics and ages of 5–100 Myr. In addition to our results for NGC 2232, we include data from Orion OB1a and b (10 and 5 Myr), Upper Centaurus Lupus (16 Myr), h and  $\chi$  Persei (13 Myr), NGC 2547 (38 Myr), IC 2602 (50 Myr), IC 2391 (50 Myr), and the Pleiades (100 Myr Hernandez et al. 2006; Currie et al. 2008a; Gorlova et al. 2007; Siegler et al. 2007; Gorlova et al. 2006).

These data demonstrate a time-dependent frequency of  $24\ \mu\text{m}$  emission from dust among young A stars (Figure 13). For stars with ages 5–25 Myr, the frequency appears to rise from  $\lesssim 40\%$  for 5–10 Myr old stars to  $\gtrsim 50\%$  for 15–25 Myr old stars. For older stars (50–100 Myr), the  $24\ \mu\text{m}$  excess frequency declines to  $\sim 10\text{--}20\%$ .

The increasing  $24\ \mu\text{m}$  excess frequency from  $\sim 5$  Myr to  $\sim 10\text{--}25$  Myr can be explained within the context of standard models of planet formation (e.g. Kenyon and Bromley 2008). During the early stages of planet formation, much of the primordial dust mass may be incorporated into  $\gtrsim$  km-sized planetesimals. This growth to larger sizes reduces the disk opacity and thus level of emission. Some disks may have undetectable levels of emission. Once forming planets reach  $\gtrsim 100\text{--}1000$  km sizes, they stir the leftover planetesimals they accrete to high velocities. When planetesimals collide with each other at these velocities, they produce copious amounts of dust which is then detectable in the mid infrared.

Next, we examine the level of  $24\ \mu\text{m}$  excess emission with respect to time (see also Rieke et al. 2005 and Currie et al. 2008a), focusing on 5–40 Myr-old early-type stars. We include the complete sample of B and A stars in NGC 2232. In addition to our data, we include stars from clusters with debris disks: Orion OB1a and b (10 and 5 Myr; Hernandez et al. 2006),  $\eta$  Cha (8 Myr; Gautier et al. 2008), the  $\beta$  Pic Moving Group (12 Myr; Rebull et al. 2008),  $\iota$  and  $\chi$  Persei ( $\sim 13$  Myr; Currie et al. 2008a), Sco-Cen, and NGC 2547 (38 Myr; Rieke et al. 2005). For the Sco-Cen, we include data for Upper Scorpius (5 Myr), Upper Centaurus Lupus (16 Myr), and Lower Centaurus Crux (17 Myr) from Chen et al. (2005a). We limit our literature sample to BAF stars.

Figure 14 shows the amplitude of  $24\ \mu\text{m}$  excess vs. time. In support of Currie et al. (2008a), there is a rise in the level of debris emission from  $\sim 5$  Myr to 10 Myr and a peak at  $\sim 10\text{--}20$  Myr<sup>8</sup>. Adding  $\gtrsim 30\text{--}50$  Myr-old clusters (Currie et al. 2008a; Rieke et al. 2005) shows that the emission is consistent with a  $1/t$  decline. The mean level of excess (dashed line) for  $\lesssim 20$  Myr-old clusters clearly deviates from a  $t^{-1}$  decline (dot-dashed line) observed for  $\gtrsim 30\text{--}50$  Myr-old stars.

These new data improve our understanding of the evolution of debris disk emission at  $\sim 20\text{--}40$  Myr. Data for NGC 2232 suggest a slow decline in debris emission from 10–20 Myr to 25 Myr. The mean level of excess emission from the  $\beta$  Pic Moving Group (12 Myr) and Sco-Cen (16–17 Myr) to NGC 2232 (25 Myr) clearly drops. However, the excess levels for NGC 2547 are comparable to those for NGC 2232. The trend in the decline of  $24\ \mu\text{m}$  excess emission is then slightly shallower than a  $1/t$  (dash-three dots) through  $\sim 30\text{--}40$  Myr. As

---

<sup>8</sup>Unpublished data for other 5–40 Myr old clusters – NGC 2362 and IC 4665 – also support this view (Currie et al. 2008d; Currie 2008b, unpublished).

shown in Kenyon and Bromley (2008), debris disk evolution models for A stars predict a high level of emission through  $\sim 30$  Myr. Debris emission declines more rapidly for sources older than  $\sim 40$ -50 Myr (Rieke et al. 2005; Su et al. 2006).

These results demonstrate that an epoch of detectable, strong mid-IR emission follows an epoch with weak or undetectable emission. When observed in an ensemble of stars at a range of ages, this sequence manifests itself as an increase of the  $24\ \mu\text{m}$  excess frequency and luminosity with respect to time. This trend is not apparent at  $8\ \mu\text{m}$  because the time for protoplanets to form in the terrestrial region probed by  $8\ \mu\text{m}$  dust emission is far shorter than in the ice giant/Kuiper belt regions which are probed by  $24\ \mu\text{m}$  dust emission (Kenyon and Bromley 2004). If  $8\ \mu\text{m}$  excess emission is systematically weaker than  $24\ \mu\text{m}$  excess, scatter in the photometry for intermediate and late-type members may conceal bona fide excess sources.

The high frequencies of  $24\ \mu\text{m}$  dust emission from multiple 10–40 Myr-old clusters imply that at least the majority of primordial disks pass through the debris disk stage at later times. Dust with emission at  $24\ \mu\text{m}$  but not at  $8\ \mu\text{m}$  probes active planet formation in regions with equilibrium temperatures of  $\approx 120$  K (Currie et al. 2008a), which is colder than the water-ice condensation temperature in the solar nebula ( $\approx 170$  K).

Within the context of the Kenyon and Bromley debris disk evolutionary models,  $24\ \mu\text{m}$  dust probes active planet formation beyond the ice line, so the frequency of icy planets around A stars ( $\approx 1.5$ -3  $M_\odot$  at this age) is  $\eta_i \approx 50$ –60%. Thus, ***most  $\approx 1.5$ –3  $M_\odot$  stars should form icy planets.***

## 6. Discussion

We have described the first search for debris disks in the 25 Myr-old nearby open cluster, NGC 2232. Using ROSAT x-ray observations and optical/IR colors and spectroscopy, we identified probable cluster members and cross correlated this list with Spitzer IRAC and MIPS data. By comparing these data with results for other 5-40 Myr old clusters, we reconstruct the time evolution of  $8\ \mu\text{m}$  and  $24\ \mu\text{m}$  emission from debris disks and probe the connection between debris emission and stellar rotation.

Our analysis identifies one A-type cluster member, HD 45435, with strong warm dust emission and 1–3 late-type stars with weakly-emitting warm dust. HD 45435 has dust with a temperature of  $T \sim 350$ –800 K and a luminosity  $L_d/L_\star \sim 5 \times 10^{-3}$ . For the late-type stars, the lack of  $24\ \mu\text{m}$  excesses yields good limits for the dust luminosity,  $L_d/L_\star \sim 1 - 10 \times 10^{-4}$ , but poor limits on the dust temperature,  $T \lesssim 200$ -300 K. The vast majority of cluster stars

lack evidence for marginal warm dust emission. Combined with results for  $\eta$  Per and NGC 2547, our analysis suggests that warm dust emission from debris disks around 10–30 Myr old stars is rare, with a frequency  $\lesssim 10\%$  (see also Mamajek et al. 2004; Currie et al. 2007a; Gorlova et al. 2007).

In contrast, cold dust emission around 10–30 Myr old A-type stars is common. Roughly half of all A stars with ages between 10 Myr and 30 Myr have excess emission at  $24\ \mu\text{m}$ . Upper limits to the excess emission at  $8\ \mu\text{m}$  yield good constraints on the dust temperature,  $T \sim \lesssim 200\text{--}300\ \text{K}$ , and luminosity,  $L_d/L_\star \lesssim 10^{-3}$ .

These results place interesting limits on the frequency of planet around young stars. For most A-type stars with  $24\ \mu\text{m}$  excesses, dust emission probes active planet formation beyond the ice line, according to debris disk evolutionary models (e.g. Kenyon and Bromley 2008). Thus, at least 50% of A-type ( $\sim 1.5\text{--}3\ M_\odot$ ) stars likely have icy planets. Warm dust emission probes terrestrial planet formation inside the ice line. Thus,  $\lesssim 10\%$  of all stars show evidence for rocky planet formation. Despite fairly large samples, it is not yet clear whether terrestrial planet formation (a) is rare, (b) produces only weak emission concealed by intrinsic photometric scatter, or (c) concludes much more rapidly than icy planet formation, as predicted by planet formation models (Kenyon and Bromley 2004).

For well-sampled clusters with ages 5–50 Myr, the frequency and magnitude of cold dust emission among early-type stars depends on stellar age. The frequency of  $24\ \mu\text{m}$  emission increases from 5–10 Myr, peaks at 10–30 Myr, and then declines. The typical amount of cold dust emission correlates with the frequency of dust emission. Both of these trends are consistent with predictions from debris disk models (Kenyon and Bromley 2004). Comparing the rotation rates of B and A stars with their  $24\ \mu\text{m}$  excesses shows that slower rotators have stronger excesses. Because primordial disk emission is also stronger for slower rotators (Cieza and Baliber 2007), there may be an evolutionary link between massive primordial disks and massive debris disks.

Despite our conclusion that icy planets are common around higher-mass stars, we cannot infer the masses of planets from the luminosity of the debris disk emission. The objects responsible for debris-producing planetesimal collisions have radii  $\gtrsim 500\ \text{km}$  and masses  $\geq 10^{-4}\ M_\oplus$ . While the debris luminosity increases as planets grow to hundreds of kilometers in size during runaway growth, the luminosity is independent of the planet size during oligarchy<sup>9</sup>. The observed  $L_d/L_\star$  depends on the initial disk mass – and thus the total mass

---

<sup>9</sup>Even though planetesimals collide at higher velocities around more massive planets, the scale height of the planetesimals also increases. Thus, the collision rate, which controls the debris luminosity, does not increase dramatically (S. Kenyon, unpublished; Kenyon and Bromley 2008)

in larger objects – more than the mass of the largest object (Kenyon and Bromley 2008).

Radial velocity surveys also constrain the frequency of planets around high-mass stars<sup>10</sup>. Current surveys show that the frequency of planets is higher around  $\geq 1.5 M_{\odot}$  stars than around solar and subsolar-mass stars (Johnson et al. 2007), consistent with theoretical expectations (Kennedy and Kenyon 2008). From the standpoint of debris disk studies, however, it is not clear whether a) high-mass stars should make more icy planets than solar-mass stars or b) high-mass stars produce more debris than they do around solar-mass stars simply because their disks are likely more massive.

This work highlights two problems that impede our understanding of terrestrial planet formation from surveys of young, open clusters with Spitzer observations. The lack of massive young clusters prevents robust constraints on terrestrial planet formation around high and intermediate-mass stars. The low luminosity of warm debris around low-mass stars limits our ability to construct large samples of stars with warm dust. High-precision photometry of nearby clusters like NGC 2232 may probe terrestrial planet formation around low-mass stars. However, NGC 2232 and most other nearby clusters are not massive enough to provide constraints on terrestrial planet formation around intermediate and high-mass stars. The only cluster studied so far that is clearly massive enough to provide robust constraints is h and  $\chi$  Persei (Currie et al. 2007a,b).

To investigate the evolution of warm debris emission around high and intermediate-mass stars more conclusively, observations of clusters more populous than NGC 2232 are necessary. Spitzer Cycle 4 and 5 observations of h and  $\chi$  Persei and other 8–20 Myr old clusters will fill this role. Preliminary analysis of MIPS h and  $\chi$  Per data taken during March 2008 show a huge increase in the number of cluster stars detected, including several terrestrial zone debris disk candidates from Currie et al. (2007b) that previously had MIPS upper limits. Observations for h and  $\chi$  Persei will be bracketed by observations of massive 8 and 20 Myr old clusters, NGC 6871 and NGC 1960, to provide better observational constraints on terrestrial planet formation during the critical 10–30 Myr epoch.

This work justifies the need for follow-up observations of NGC 2232. New optical photometry, spectroscopy, and x-ray surveys will provide a far better constraint on cluster membership and member properties, which will improve the utility of NGC 2232 as a laboratory for studying debris disk evolution and planet formation. Lyra et al. (2006) showed that optical colors provide a useful diagnostic of cluster membership; a deep spectroscopic survey to identify late-type members is also feasible with multi-object spectrographs like Hectospec

---

<sup>10</sup>However, constraining the frequency of *icy* planets around high-mass stars requires an observing baseline that is much longer than that which is currently available.

on the MMT and Hydra at Kitt Peak. Identifying late-type members with a deep Chandra survey of NGC 2232 would better constrain the evolution of x-ray activity from 10 Myr to 50 Myr in addition to identifying late-type, chromospherically active cluster stars. All these observations should provide a much more complete census of cluster members, which in turn will yield a better analysis of the disk population for late-type stars.

Finally, the proximity of NGC 2232 to the Sun allows for follow-up ground-based/space-based observations of disks, some of which are not possible with distant, populous clusters such as  $\eta$  and  $\chi$  Persei, NGC 6871, and NGC 1960. The hot dust emission from ID 18566 may be resolvable by ground-based interferometers such as the Large Binocular Telescope Interferometer. The ESO space telescope *Herschel* should be able to survey NGC 2232 for evidence of cold debris disks emitting longwards of  $\sim 40 \mu m$ . With a significant disk population established, NGC 2232 should be an excellent target for mid-IR observations with the *James Webb Space Telescope*.

Although NGC 2232 has been virtually ignored by the star/planet formation community for the past 30 years, this work shows it to be a potentially important laboratory for understanding debris disk evolution and planet formation which deserves further study.

We thank the anonymous referee for a thorough review and helpful suggestions which improved the quality of this paper. We also thank Nancy Remage Evans for advice on ROSAT archival data and Jesus Hernandez for use of the SPTCLASS spectral-typing code. Finally, we thank Ken Rines for taking a spectrum of ID 18012 on short notice. This work is supported by Spitzer GO grant 1320379, NASA Astrophysics Theory grant NAG5-13278, and NASA grant NNG06GH25G. This paper makes use of the WEBDA open cluster database.

## REFERENCES

- Augereau, J. C., Lagrange, A. M., Mouillet, D., Papaloizou, J. C. B., Grorod, P. A., 1999, *A&A*, 348, 557
- Backman, D., Paresce, F., 1993, in *Protostars and Planets III* (E.H. Levy and J.I. Lunine, eds.) (Univ. of Arizona, Tucson), 1253, (1993)
- Baraffe, I., et al., 1998, *A&A*, 337, 403
- Bertin, E., & Arnouts, S., 1996, *A&AS*, 117, 393
- Bouvier, J., Cabrit, S., Fernandez, M., Martin, E. L., & Matthews, J. M., 1993, *A&A*, 26, 272

- Bouvier, J., Forestini, M., Allain, S., 1997, *A&A* 326, 1023
- Bouwman, J., et al., 2008, *ApJ* accepted, arXiv:0802.3033
- Calvet, N., et al., 2005, *ApJ*, 630, 185L
- Carpenter, J., Mamajek, E., Hillenbrand, L., Meyer, M., 2006, *ApJ*, 651, 49L
- Chen, C., Jura, M., Gordon, K. D., Blaylock, M., 2005, *ApJ*, 623, 493
- Chen, C., et al., 2006, *ApJS*, 166, 351
- Cieza, L., Baliber, N., 2007, *ApJ*, 671, 605
- Claria, J., 1972, *A&A*, 19, 309
- Currie, T., et al., 2007, *ApJ*, 659, 599
- Currie, T., Evans, N., et al., 2008, *AJin prep.*
- Currie, T., Kenyon, S., Rieke, G., Balog, Z., Bromley, B., 2007, *ApJ*, 663, 105L
- Currie, T., Kenyon, S., Balog, Z., Bragg, A., Tokarz, S., 2007, *ApJ*, 669, 33L
- Currie, T., Kenyon, S., Balog, Z., Rieke, G., Bragg, A., Bromley, B., 2008, *ApJ*, 672, 558
- Currie, T., et al., 2008, in prep.
- Currie, T., 2008, Ph.D. thesis, University of California-Los Angeles
- Currie, T., Kenyon, S. J., 2008, submitted, arXiv:0801.1116
- Currie, T., Irwin, J., Hernandez, J., et al., 2008, in prep.
- Fabricant, D., et al., 1998, *PASP*, 110, 79
- Fazio, G., et al., 2004, *ApJS*, 154, 10
- Gautier, T., et al., 2007, *ApJ*, 667, 527
- Gautier, T., et al., 2008, *ApJ* accepted, arXiv:0804.3113
- Gorlova, N., et al., 2006, *ApJ*, 649, 1028
- Gorlova, N., Balog, Z., Rieke, G. H., Muzerolle, J., Su, K. Y. L., Ivanov, V. D., Young, E. T., 2007, *ApJ*, 670, 516

- Herbst, W., Bailer-Jones, C. A. L., & Mundt, R. 2001, *ApJ*, 554, 197L
- Hernandez, J., Calvet, N., Briceno, C., Hartmann, L., Berlind, P., 2004, *AJ*, 127, 1682
- Hernandez, J., Briceno, C., Calvet, N., Hartmann, L., Muzerolle, J., & Quintero, A., 2006, *ApJ*, 652, 472
- Hernandez, J., et al., 2007, *ApJ*, 662, 1067
- Hillenbrand, L., 2005, *astro-ph/0511083*
- Hillenbrand, L., et al., 2008, *ApJ*, 677, 630
- Indebetouw, R., et al., 2005, *ApJ*, 619, 9311
- Irwin, J., et al., 2008, *MNRAS*, 384, 675
- Jacoby, G., et al., 1984, *ApJS*, 56, 257
- Johnson, J., et al., 2007, *ApJ*, 670, 833
- Kennedy, G., Kenyon, S. J., 2008, *ApJ*, 673, 502
- Kenyon, S., Bromley, B., 2004, *ApJ*, 602, 133L
- Kenyon, S., Bromley, B., 2006, *AJ*, 131, 1837
- Kenyon, S., Bromley, B., 2008, *ApJS*, submitted
- Kenyon, S., Hartmann, L., 1987, *ApJ*, 323, 714
- Kenyon, S., Hartmann, L., 1995, *ApJS*, 101, 117
- Kurucz, R. L., 1993, *SYNTHE Synthesis Programs and Line Data Kurucz CD-ROM No. 18*, Cambridge, MA: Smithsonian Astrophysical Observatory, 1993, 18
- Lada, C. J., et al., 2006, *AJ*, 131, 1574
- Lejeune, Th., Cuisinier, F., and Buser, R., 1997, *A&AS*, 125, 229
- Levato, H., Malaroda, S., 1974, *AJ*, 79, 890
- Levato, H., 1974, *AJ*, 79, 1269
- Lisse, C., Chen, C., Wyatt, M., Morlock, A., 2008, *ApJ*, 673, 1106

- Low, F., Smith, P., Werner, M., Chen, C., Krause, V., Jura, M., Hines, D., 2005, *ApJ*, 631, 1170
- Lyra, W., et al., 2006, *A&A*, 453, 101
- Makidon, R. B., Rebull, L. M., Strom, S. E., Adams, M. T., & Patten, B. M., 2004, *AJ*, 127, 2228
- Mamajek, E., et al., 2004, *ApJ*, 612, 496
- Mathis, J., 1990, *ARA&A*, 28, 37
- Mayne, N. J., Naylor, T., 2008, *MNRAS* accepted, arXiv:0801.4085
- Meyer, M., et al., 2006, *PASP*, 118, 1690
- Naylor, T., Jeffries, R. D., 2006, *MNRAS*, 373, 1251
- Padgett, D., et al., 2006, *ApJ*, 645, 1283
- Panzer, M. R., Campana, S., Covino, S., Lazzati, D., Mignani, R. P., Moretti, A., Tagliaferri, G., 2003, *A&A*, 399, 351
- Papovich, C., et al., 2004, *ApJS*, 154, 70
- Plavchan, P., et al., 2005, *ApJ*, 631, 1161
- Plavchan, P., et al., 2008, in prep.
- Preibisch, T., Feigelson, E., 2005, *ApJS*, 160, 390
- Quijada, M., et al., 2004, *SPIE*, 5487, 244
- Rebull, L., Wolff, S. C., & Strom, S. E. 2004, *AJ*, 127, 1029
- Rebull, L., et al., 2006, *ApJ*, 646, 297
- Rebull, L., et al., 2008, *ApJ* in press, arXiv:0803.1674
- Rhee, J., Song, I., Zuckerman, B., McElwain, M., 2007, *ApJ*, 660, 1556
- Rhee, J., Song, I., Zuckerman, B., 2007, *ApJ*, 671, 166
- Rhee, J., Song, I., Zuckerman, B., 2008, 675, 777
- Rieke, G., et al., 2004, *ApJS*, 154, 25

- Rieke, G., 2005, ApJ, 620, 1010
- Rieke, G., et al., 2008, AJ, 135, 2245
- Sargent, B., et al., 2006, ApJ, 645, 395
- Shu, F., et al., 1994, ApJ, 429, 781
- Siegler, N., et al., 2007, ApJ, 654, 580
- Siess, L., Dufour, E., Forestini, M., 2000, A&A, 358, 593
- Song, I., Zuckerman, B., Weinberger, A., Becklin, E., 2005, Nature, 436, 363
- Stauffer, J., et al., 2005, AJ, 130, 1834
- Staussun, K. G., Mathieu, R. D., Mazeh, T., & Vrba, F. J. 1999, AJ, 117, 2941
- Su, K., et al., 2006, ApJ, 653, 675
- Voges, W., et al., 1999, A&A, 349, 389
- Werner, M., et al., 2004, ApJS, 154, 1
- Wetherill, G., Stewart, G., 1993, Icarus, 106, 190
- White, R., Basri, G., 2003, ApJ, 582, 1109
- Wyatt, M., et al., 2007, ApJ, 658, 569
- Yin, Q., et al., 2002, Nature, 418, 949
- Zuckerman, B., Song, I., 2004, ARA&A, 42, 685

Table 1. Photometry Catalogue for Sources with Detected on NGC 2232 field

| ID | RA      | DEC     | V    | J     | H     | K <sub>s</sub> | [3.6] | $\sigma$ ([3.6]) | [4.5] | $\sigma$ ([4.5]) | [5.8] | $\sigma$ ([5.8]) | [8]  | $\sigma$ ([8]) | [24]  | $\sigma$ ([24]) |
|----|---------|---------|------|-------|-------|----------------|-------|------------------|-------|------------------|-------|------------------|------|----------------|-------|-----------------|
| 1  | 96.4706 | -5.3994 | 0.00 | 13.51 | 13.05 | 12.86          | 0.00  | -99.00           | 0.00  | -99.00           | 0.00  | -99.00           | 0.00 | -99.00         | 10.25 | 0.15            |
| 2  | 96.4708 | -5.4639 | 0.00 | 11.19 | 10.46 | 10.19          | 0.00  | -99.00           | 0.00  | -99.00           | 0.00  | -99.00           | 0.00 | -99.00         | 9.78  | 0.14            |
| 3  | 96.4790 | -5.1864 | 0.00 | 15.82 | 15.12 | 14.90          | 0.00  | -99.00           | 0.00  | -99.00           | 0.00  | -99.00           | 0.00 | -99.00         | 9.22  | 0.06            |
| 4  | 96.4816 | -5.3179 | 0.00 | 10.52 | 9.91  | 9.71           | 0.00  | -99.00           | 0.00  | -99.00           | 0.00  | -99.00           | 0.00 | -99.00         | 9.66  | 0.09            |
| 5  | 96.4836 | -5.0643 | 0.00 | 9.90  | 9.67  | 9.56           | 0.00  | -99.00           | 0.00  | -99.00           | 0.00  | -99.00           | 0.00 | -99.00         | 9.68  | 0.09            |

Note. — The table includes sources with at least one detection in a Spitzer IRAC or MIPS band. Values of 0.00 in the photometry column and -99.00 in the photometric uncertainty columns denote sources that were not observed in a given filter. Sources observed in the MIPS band but not in the IRAC bands fall outside the IRAC coverage.

Table 2. Spectroscopy of Selected NGC 2232 sources

| ID    | RA      | DEC     | Spectral Type | $\sigma$ (Spectral Type) | EW(H $\alpha$ ) | FWHM(H $\alpha$ ) | ROSAT counts ks <sup>-1</sup> | Member? |
|-------|---------|---------|---------------|--------------------------|-----------------|-------------------|-------------------------------|---------|
| 1050  | 96.5720 | -4.5989 | G0.7          | 3.4                      | 2.70            | 99                | –                             | no      |
| 6041  | 96.8377 | -4.9424 | G6.3          | 2.4                      | 2.40            | 99                | –                             | no      |
| 6639  | 96.8691 | -4.8748 | G3.7          | 2.0                      | 0.00            | 99                | –                             | no      |
| 10258 | 97.0566 | -4.5612 | K6.0          | 1.2                      | 1.60            | 99                | –                             | yes     |
| 10763 | 97.0836 | -4.6977 | G2.5          | 2.6                      | 2.00            | 99                | –                             | yes     |
| 16505 | 97.3680 | -4.6234 | F4.0          | 1.4                      | 4.50            | 99                | –                             | no      |
| 18012 | 97.4388 | -5.0088 | M0.0          | 1.5                      | -0.7            | 99                | –                             | yes     |
| 18553 | 96.8783 | -4.6588 | F9.8          | 1.9                      | 2.30            | 99                | 6.1                           | yes     |
| 18554 | 96.6436 | -4.5974 | B3.1          | 1.3                      | 5.90            | 99                | 1.4                           | yes     |
| 18555 | 96.8426 | -4.5690 | K1.8          | 1.2                      | -0.15           | 99                | 2.1                           | yes     |
| 18558 | 96.7537 | -4.3556 | B3.9          | 1.4                      | 5.90            | 99                | 0.9                           | yes     |
| 18559 | 96.6810 | -4.7450 | F5.0          | 3.0                      | 5.00            | 99                | 1.5                           | yes     |
| 18560 | 96.5763 | -4.5993 | M3.2          | 0.9                      | -7.40           | 5.20              | 0.9                           | yes     |
| 18562 | 96.6217 | -4.3049 | M3.6          | 1.0                      | -6.90           | 5.00              | 0.7                           | yes     |
| 18566 | 96.7940 | -4.7801 | A2.8          | 2.5                      | 9.90            | 99                | 1.5                           | yes     |
| 18568 | 97.0254 | -4.6412 | M0.8          | 0.7                      | -1.80           | 4.30              | 0.9                           | yes     |
| 18570 | 96.8788 | -4.5815 | M3.1          | 0.8                      | -5.10           | 5.40              | 1.2                           | yes     |
| 18572 | 96.8402 | -4.9407 | F7.3          | 2.3                      | 3.90            | 99                | 2.6                           | no      |
| 18577 | 97.0173 | -4.8984 | K3.9          | 1.2                      | -0.76           | 5.90              | 3.6                           | no      |
| 18578 | 96.8713 | -4.8730 | M3.6          | 0.9                      | -6.30           | 6.00              | 1.3                           | yes     |
| 18579 | 96.9484 | -4.8247 | B7.6          | 1.2                      | 7.20            | 99                | 2.1                           | yes     |
| 18580 | 97.0004 | -4.7930 | M2.9          | 1.2                      | -3.70           | 4.50              | 0.8                           | yes     |
| 18581 | 96.9899 | -4.7621 | B0.8          | 1.4                      | 4.60            | 99                | 5.9                           | yes     |
| 18582 | 96.8650 | -4.7564 | M0.8          | 0.8                      | -1.80           | 6.00              | 1.9                           | yes     |
| 18587 | 97.1874 | -4.7139 | M0.5          | 0.8                      | -2.28           | 4.70              | 2.2                           | yes     |
| 18590 | 96.9365 | -4.7342 | M4.2          | 1.1                      | -8.80           | 5.70              | 0.6                           | yes     |
| 18599 | 96.9009 | -4.9428 | M3.5          | 1.0                      | -5.10           | 5.30              | 0.8                           | yes     |
| 18605 | 97.1404 | -4.7829 | G1.4          | 2.5                      | 2.80            | 99                | 1.0                           | yes     |
| 18606 | 96.9688 | -4.7669 | B9.5          | 1.3                      | 11.10           | 99                | 0.4                           | yes     |
| 18607 | 97.0515 | -4.7617 | M3.9          | 1.2                      | -7.00           | 5.00              | 0.5                           | yes     |
| 18612 | 97.0250 | -4.6057 | M2.4          | 0.7                      | -5.05           | 5.20              | 1.2                           | yes     |
| 18613 | 97.0584 | -4.5622 | K7.5          | 0.8                      | -1.50           | 6.30              | 1.5                           | yes     |
| 18617 | 97.0399 | -4.7984 | M2.0          | 0.8                      | -3.80           | 5.10              | 1.1                           | yes     |
| 18620 | 97.0354 | -4.7400 | M2.2          | 0.8                      | -9.25           | 5.50              | 0.6                           | yes     |
| 18621 | 96.9177 | -4.7127 | M3.7          | 1.2                      | -6.06           | 4.90              | 2.1                           | yes     |
| 18622 | 97.0234 | -4.6411 | M3.4          | 1.1                      | -8.20           | 5.80              | 2.6                           | yes     |
| 18633 | 96.5333 | -4.6282 | B8.8          | 1.2                      | 8.80            | 99                | –                             | yes     |

Note. — FAST spectra of selected stars in the NGC 2232 field. ID 10258 has a near-IR colors lying just outside the range for candidate members but a spectral type possibly consistent with membership. The uncertainties in spectral type ( $\sigma$ (ST)) are determined from the dispersion in spectral types computed from each of the spectral indices (see Hernandez et al. 2004, for more information). Entries in the FWHM(H $\alpha$ ) column with a value of '99' did not have H $\alpha$  clearly in emission and/or a high enough signal to noise to calculate a reliable full-width half-maximum.

Table 3. Confirmed and Candidate Cluster Members with Spitzer Data

| ID   | RA      | DEC     | Mem. Type |
|------|---------|---------|-----------|
| 150  | 96.5238 | -4.7164 | 4         |
| 845  | 96.5620 | -4.6887 | 4         |
| 964  | 96.5676 | -4.4612 | 4         |
| 985  | 96.5687 | -4.4479 | 4         |
| 1084 | 96.5738 | -4.8108 | 4         |

Note. — The table includes sources with at least one detection in a Spitzer IRAC or MIPS band. Membership type 1 denotes confirmed x-ray active cluster members; type 2 identifies members from Claria (1972). Type 3 lists ‘candidate’ members as determined from V/V-J colors, spectroscopy, and proper motion. Type 4 lists ‘candidate’ members determined from J/J-K<sub>s</sub> and J/J-H colors.

Table 4. Photospheric 2MASS-IRAC/MIPS Colors

| Spectral Type | K <sub>s</sub> -[5.8] | K <sub>s</sub> -[8] | K <sub>s</sub> -[24] |
|---------------|-----------------------|---------------------|----------------------|
| B0            | -0.17                 | -0.24               | -0.34                |
| B3            | -0.11                 | -0.16               | -0.21                |
| B5            | -0.07                 | -0.12               | -0.1                 |
| B8            | -0.05                 | -0.1                | -0.1                 |
| A0            | -0.02                 | -0.05               | -0.1                 |
| A5            | -0.01                 | -0.05               | -0.1                 |
| F0            | 0.02                  | -0.02               | 0.005                |
| F5            | 0.02                  | -0.02               | 0.005                |
| G0            | 0.01                  | -0.02               | 0.005                |
| G5            | 0.01                  | -0.02               | 0.005                |
| K0            | 0.01                  | 0                   | 0.005                |
| K5            | 0.08                  | 0.1                 | 0.1                  |
| M0            | 0.21                  | 0.24                | 0.34                 |
| M2            | 0.25                  | 0.30                | 0.41                 |
| M5            | 0.28                  | 0.33                | 0.41                 |

Table 5. 8 $\mu$ m Excess Sources in NGC 2232

| ID    | Cross-ID | Spectral Type | $\log(F_{[8]}/F_{[4.5]})$ | $\log(F_{[8]}/F_{[4.5]})$ -Photosphere | Excess/ $\sigma_{rms}$ |
|-------|----------|---------------|---------------------------|--|------------------------|
| 6540  | –        | K5-M0         | -0.262                    | 0.163                                  | 9.61                   |
| 9220  | –        | K7-M2         | -0.349                    | 0.074                                  | 4.39                   |
| 18566 | HD 45435 | A2.8          | -0.168                    | 0.292                                  | 17.24                  |
| 18613 | –        | K2-K7         | -0.355                    | 0.074                                  | 4.35                   |

Note. — Sources with warm, 8  $\mu$ m excess emission from circumstellar dust as determined by their 8  $\mu$ m to 4.5  $\mu$ m flux ratios. Sources with a range of spectral types have this range estimated photometrically. Two other sources, IDs 18601 and 18622, have K<sub>s</sub>-[8] colors that are greater than 3 $\sigma_{[8]}$  away from photospheric predictions. However, these sources do not have [8]/[4.5] flux ratios that are more than 3 $\sigma$  away from the empirically-determined locus of photospheric ratios.

Table 6. Early-Type Members and Intermediate/Late-Type Members with  $24\ \mu\text{m}$  Excess

| ID    | Cross-ID           | Spectral Type | $K_s-[8]$ | $K_s-[24]$ | $24\ \mu\text{m}$ Excess? | $V \sin i$ (km s $^{-1}$ ) |
|-------|--------------------|---------------|-----------|------------|---------------------------|----------------------------|
| 18554 | HD 45321           | B3.1          | -0.21     | -0.23      | no                        | 245                        |
| 18558 | HD 45418, 9 Mon    | B3.9          | -0.23     | -0.21      | no                        | 230                        |
| 18566 | HD 45435           | A2.8          | 1.00      | 2.24       | yes                       | 155                        |
| 18579 | HD 45516           | B7.6          | -0.13     | -0.08      | no                        | 270                        |
| 18581 | HD 45546           | B0.8          | -0.19     | 0.04       | no                        | 45                         |
| 18606 | BD-04 1526B        | B9.5          | -0.05     | –          | no data                   | –                          |
| 18616 | –                  | –             | -0.13     | -0.13      | no                        | –                          |
| 18630 | HD 45583, V682 Mon | B8            | -0.17     | -0.06      | no                        | 70                         |
| 18631 | HD 45532           | A0            | -0.04     | -0.11      | no                        | 320                        |
| 18633 | HD 45238           | B8.8          | -0.02     | 0.27       | yes                       | 390                        |
| 18634 | HD 45399           | A0            | -0.05     | 0.80       | yes                       | 170                        |
| 18635 | HD 295102          | B8            | -0.04     | 0.53       | yes                       | $\leq 40$                  |
| 18636 | HD 45627           | A0            | -0.04     | 0.40       | yes                       | 50                         |
| 18638 | HD 45565           | A0            | -0.08     | 1.00       | yes                       | 60                         |
| 18639 | HD 45691           | A0            | 0.0       | 1.50       | yes                       | 75                         |
| 18648 | HD 295100          | A7-F2         | -0.07     | 0.37       | yes                       | –                          |
| 4144  | –                  | G2-G7         | -0.07     | 0.39       | yes                       | –                          |
| 5494  | –                  | F2-F7         | –         | 0.75       | yes                       | –                          |
| 18012 | –                  | M0            | 0.21      | 1.57       | yes                       | –                          |

Note. — Spectral types come from the VIZIER database except those determined in this work. Sources with a range of spectral types have this range estimated from their  $J-K_s$  colors. ID 4144 is identified as a candidate member from its position on the  $J/J-H$  and  $J/J-K_s$  color-magnitude diagrams. ID 5494 is identified as a candidate member from its position on the  $V/V-J$ ,  $J/J-H$ , and  $J/J-K_s$  color-magnitude diagrams. ID 18012 is identified as a candidate member from the  $J/J-H$  and  $J/J-K_s$  diagrams and then confirmed as a member spectroscopically.

Table 7. Frequency of  $8\mu\text{m}$  Excess from  $\gtrsim 10$  Myr-old Clusters

| Cluster             | Age | Parent Sample Size | Freq. BA       | Freq. FG          | Freq. KM         | References |
|---------------------|-----|--------------------|----------------|-------------------|------------------|------------|
| h and $\chi$ Persei | 13  | 4,700              | 1.3% (14/1023) | 6.5% (34/523)     | –                | 1          |
|                     |     |                    | 2.2% (42/1878) | 8% (50/618)       | –                |            |
| NGC 2232            | 25  | 238                | 6.7% (1/15)    | 0 (0/33)          | 0-1.9% (0-3/158) | 2          |
| NGC 2547            | 38  | 450                | 0 (0/19)       | 1.6-4.9% (1-3/62) | 1-2.3% (3-8/347) | 3          |

Note. — References are 1) Currie et al. (2007a); Currie (2008), 2) this work, and 3) Gorlova et al. (2007). Parent sample size refers to the initial photometric sample. The sizes of individual subsets are listed in parentheses in columns 4-6. Values for the fraction of excess sources in NGC 2547 include an estimate on the fraction of interloping intermediate/late-type sources that are not likely to be proper motion members. Values for h and  $\chi$  Persei include the sample of sources that are photometrically consistent with cluster membership as well as a subset with spectra. The frequency of  $8\ \mu\text{m}$  excess around late-type stars for NGC 2232 is highly uncertain due to the incomplete membership list.

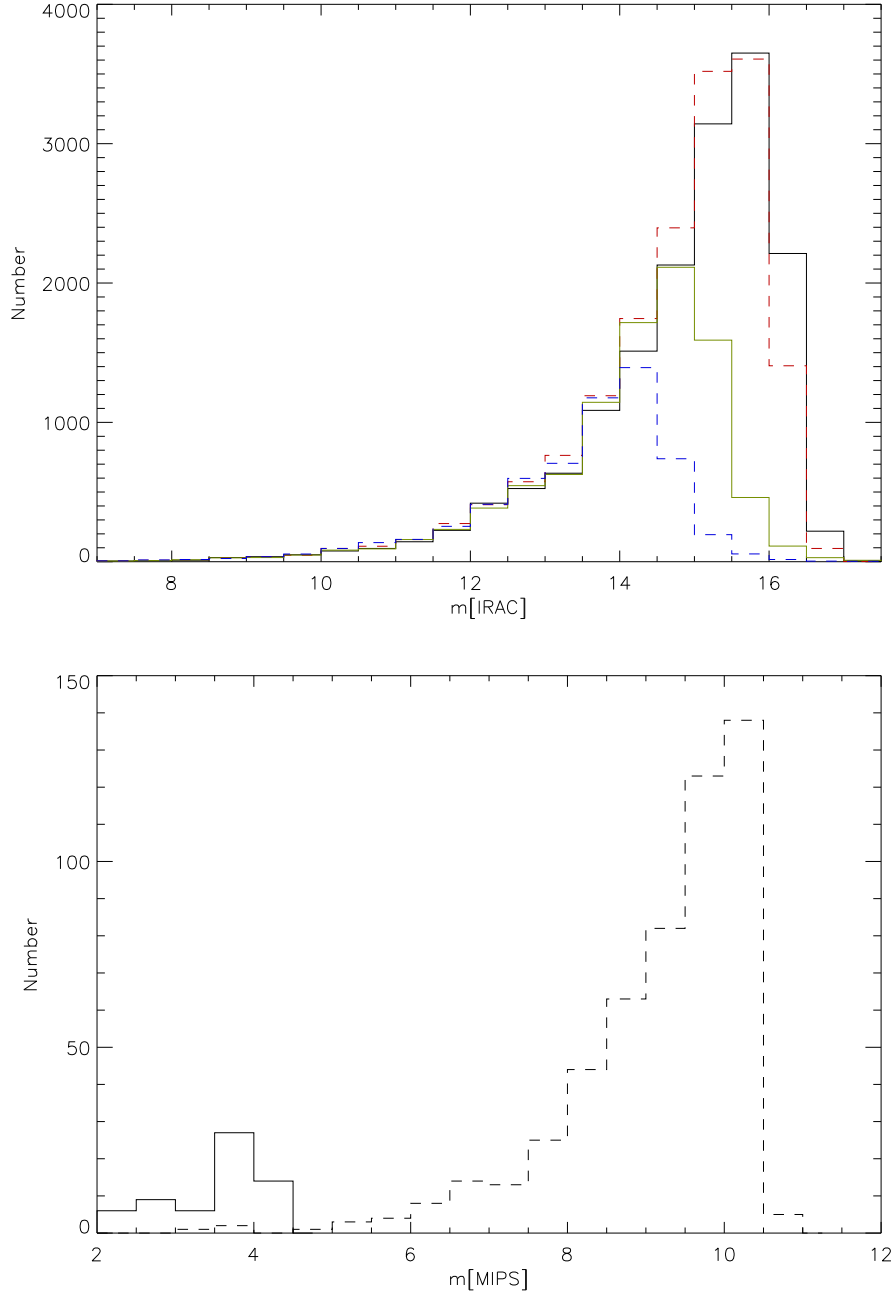


Fig. 1.— (Top) Distribution of IRAC detections with 2MASS counterparts. From right to left, the distributions are for the [3.6], [4.5], [5.8], and [8] channels. The source counts peak at a magnitude of 16, 16, 15, and 14.5 for the [3.6], [4.5], [5.8], and [8] channels, respectively. (Bottom) Distribution of MIPS  $24\ \mu\text{m}$  and  $70\ \mu\text{m}$  detections with 2MASS counterparts. The number counts in the  $24\ \mu\text{m}$  filter peak at  $[24] \sim 10.5$  while those in the  $70\ \mu\text{m}$  filter peak at  $[70] \sim 4$ .

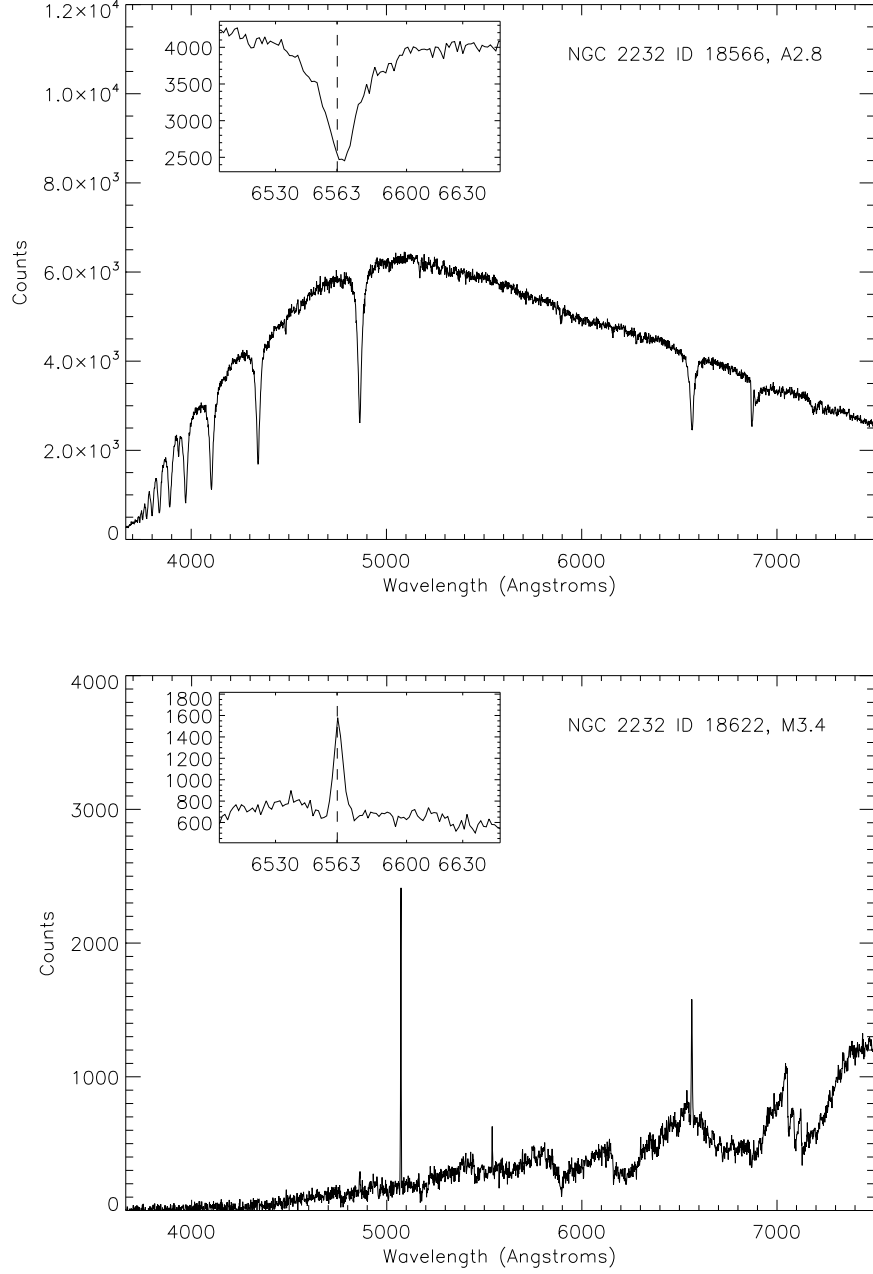


Fig. 2.— Spectra of NGC 2232 cluster members ID 18566 and ID 18662. Both sources have very red  $K_s$ -[5.8] and  $K_s$  - [8] colors. The insert show the H $\alpha$  line profile.

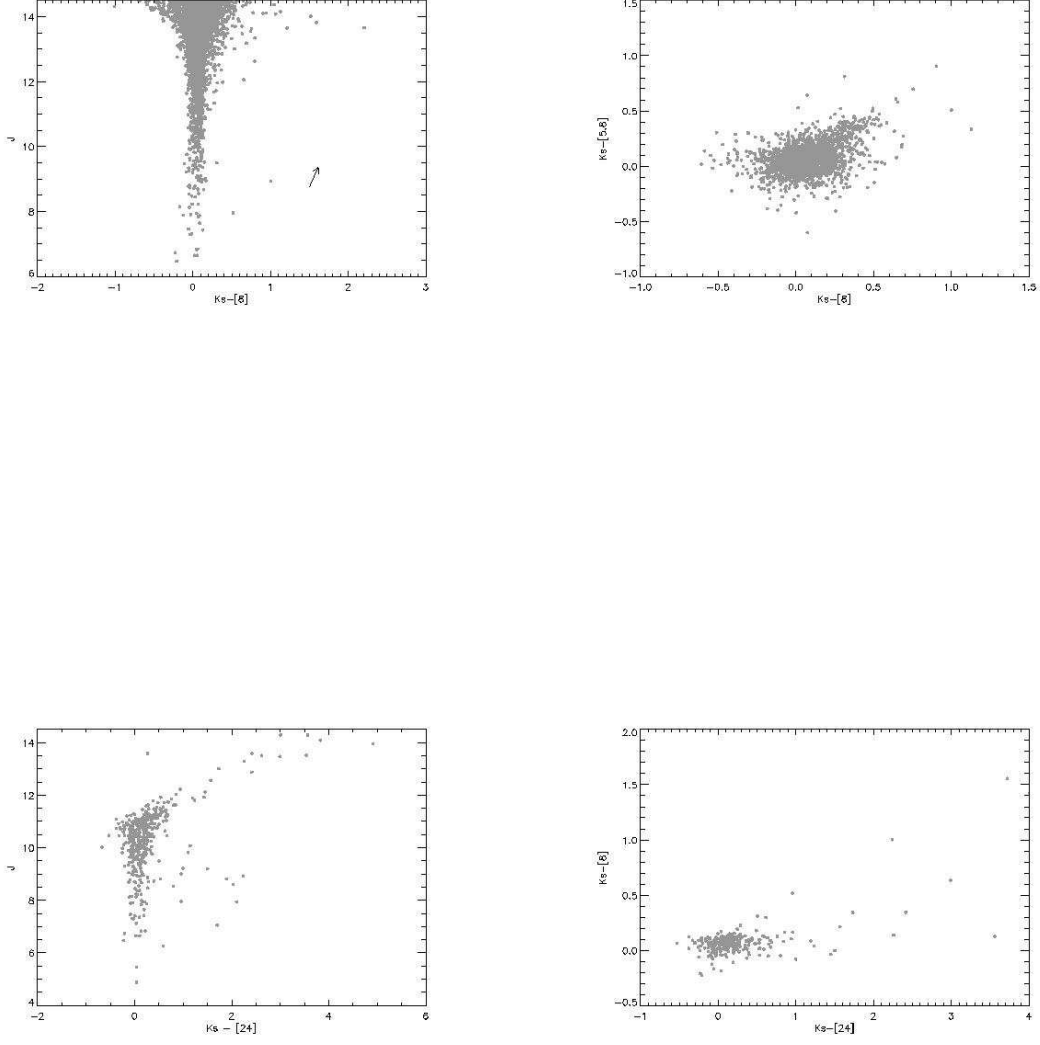


Fig. 3.— Color-magnitude and color-color diagrams for NGC 2232. Top left:  $J$  vs.  $K_s - [8]$  color-magnitude diagram. Top right:  $K_s - [5.8]/K_s - [8]$  color-color diagram. Bottom left:  $J$  vs.  $K_s - [24]$  color-magnitude diagram. Bottom right:  $K_s - [8]/K_s - [24]$  color-color diagram. The reddening vector is derived from the reddening laws derived by Indebetouw et al. (2005)

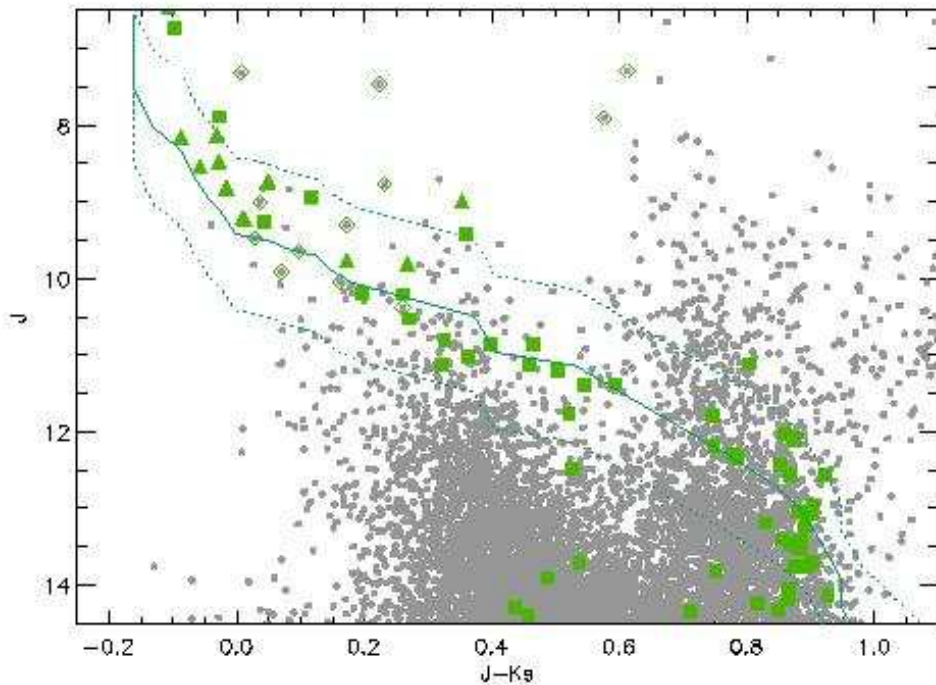


Fig. 4.—  $J/J-K_s$  color-magnitude diagram identifying probable cluster members in NGC 2232. Green triangles denote x-ray quiet cluster members identified by Claria (1972); green squares identify x-ray active sources. Stars rejected as non members by Claria (1972) are shown as grey dots surrounded by open diamonds. The sequence of x-ray quiet cluster

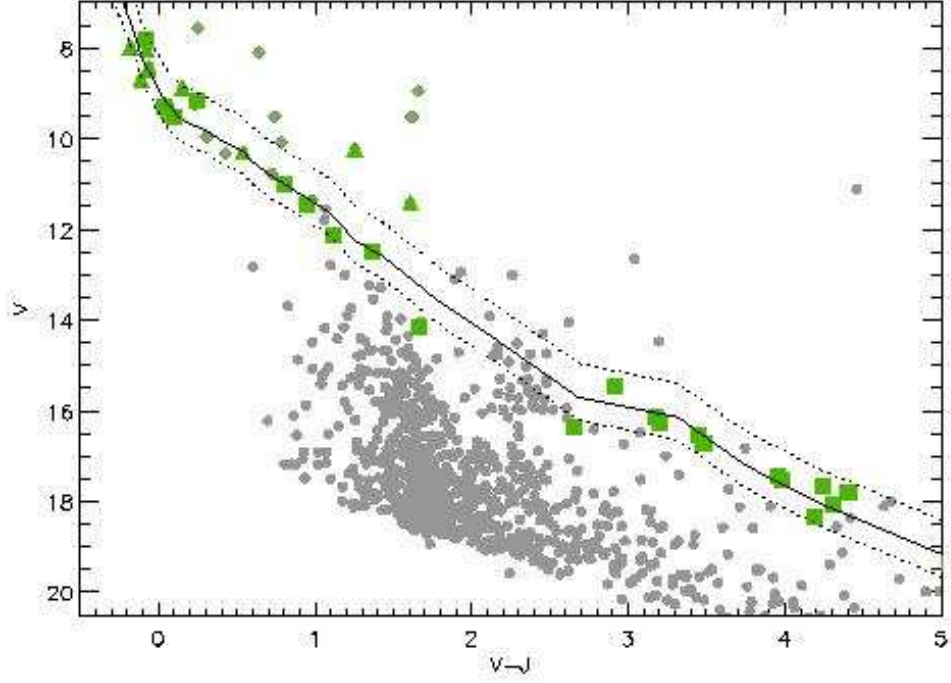


Fig. 5.—  $V/V-J$  color-magnitude diagram showing the positions of x-ray active cluster members and bright members compared with other stars. Symbols and lines as in Figure 4. The cluster members define a clear locus in  $V/V-J$ .

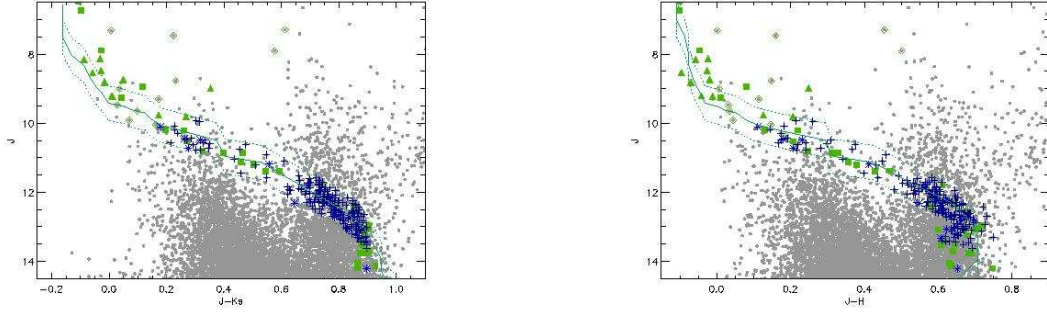


Fig. 6.—  $J/J-H$  and  $J/J-K_s$  color-magnitude diagrams showing positions of confirmed and candidate cluster members. Sources from the Claria (1972) catalog (triangles) and ROSAT detections (squares) are 'confirmed' members. Candidate members were selected based on  $V/V-J$  (asterisks) and  $J/J-H$  and  $J/J-K_s$  (crosses) color-magnitude diagrams.

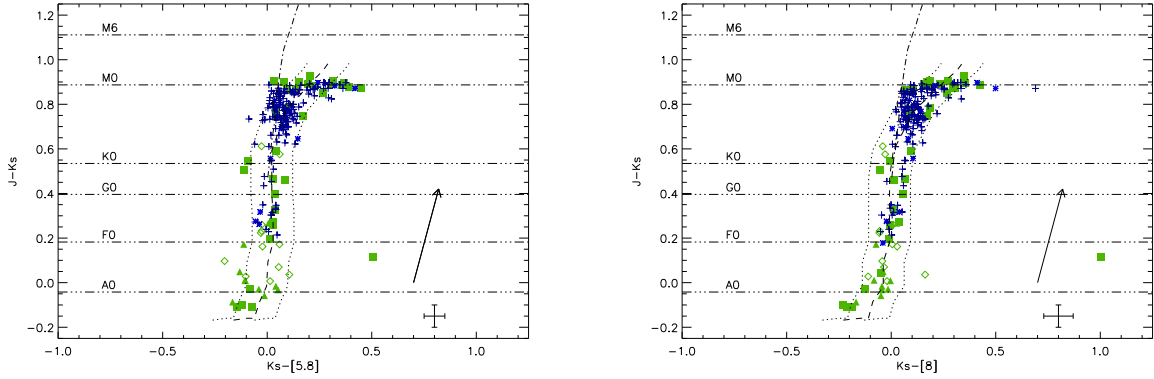


Fig. 7.—  $J-K_s$  vs.  $K_s-[5.8]$  and  $K_s-[8]$  for NGC 2232 cluster members and field stars in the Claria (1972) catalog. The symbols are the same as in the previous figures. Most members shown are ‘candidate’ members selected from their positions on the  $J/J-K_s$  and  $J/J-H$  color-magnitude diagrams. We also show the  $J-K_s$  colors expected for star with a range of spectral types (dash-three dots). The maximum photometric errors are shown in the lower right-hand corner. Most faint sources have  $\sigma[5.8,8] \sim 0.02-0.04$ . There are 1-2 sources with blue  $J-K_s$  colors and  $[5.8]$  and  $[8]$  excess; a second potential population of excess sources is centered on  $J-K_s \sim 0.85$  and has  $K_s-[5.8, 8] \lesssim 0.3-0.4$ .

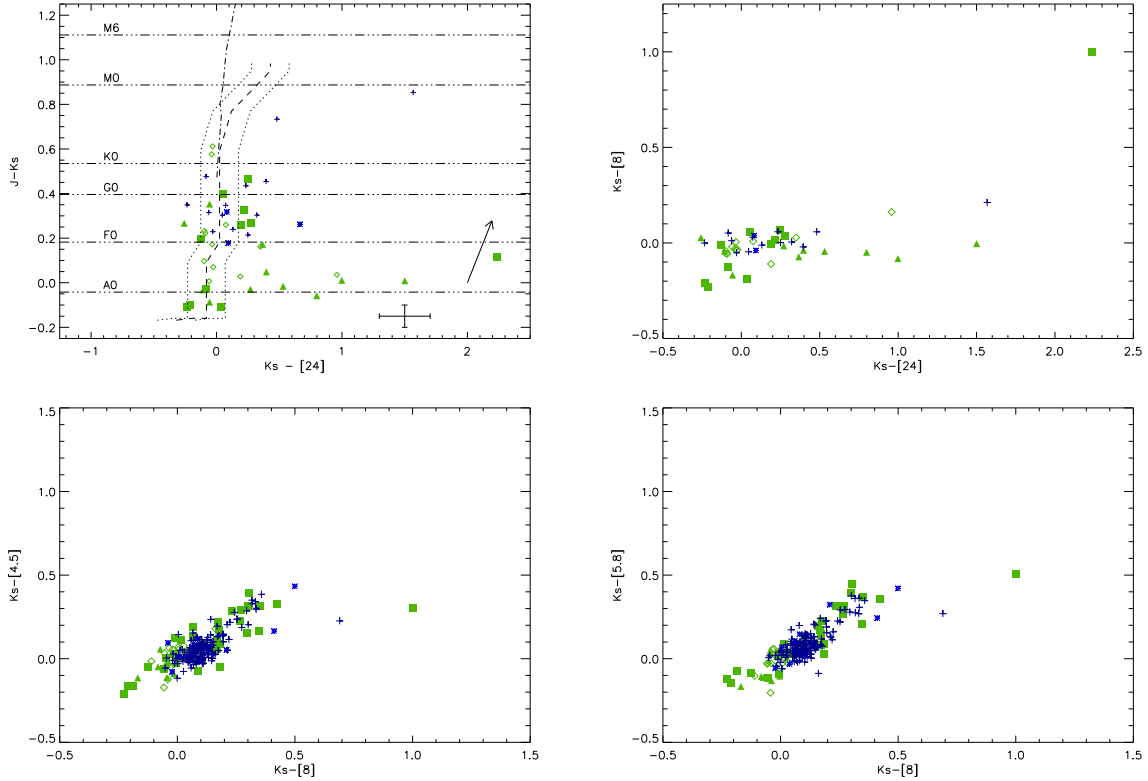


Fig. 8.— Color-color diagrams for cluster members and Claria (1972) field stars. The symbols are the same as in previous figures. (top left)  $J-K_s$  vs.  $K_s-[24]$  colors: many cluster members have  $24\ \mu m$  excesses. (top right)  $K_s-[8]$  vs.  $K_s-[24]$  colors for members and field stars. With one exception, the sources with clear MIPS excesses have photospheric IRAC colors. (bottom)  $K_s-[4.5]$  and  $K_s-[5.8]$  vs.  $K_s-[8]$  color-color diagrams. Almost all sources lie in a locus consistent with photospheric colors from early to late-type stars. The spectral types shown in the top-left panel (dash-three dots) are derived from Siess et al. (2000) using the color conversions from Kenyon and Hartmann (1995).

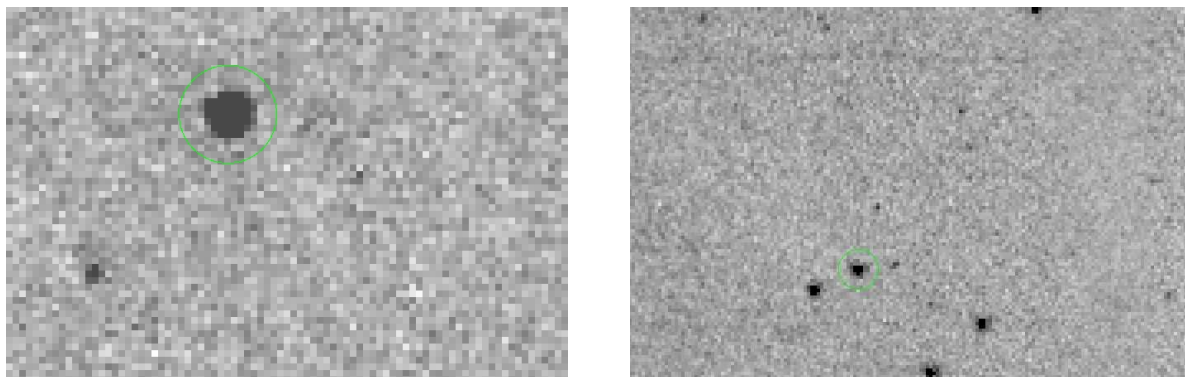


Fig. 9.— IRAC images of ID 18566 (left) and ID 18601 (right). Neither sources show evidence for source blending that could artificially brighten them in the IRAC bands.

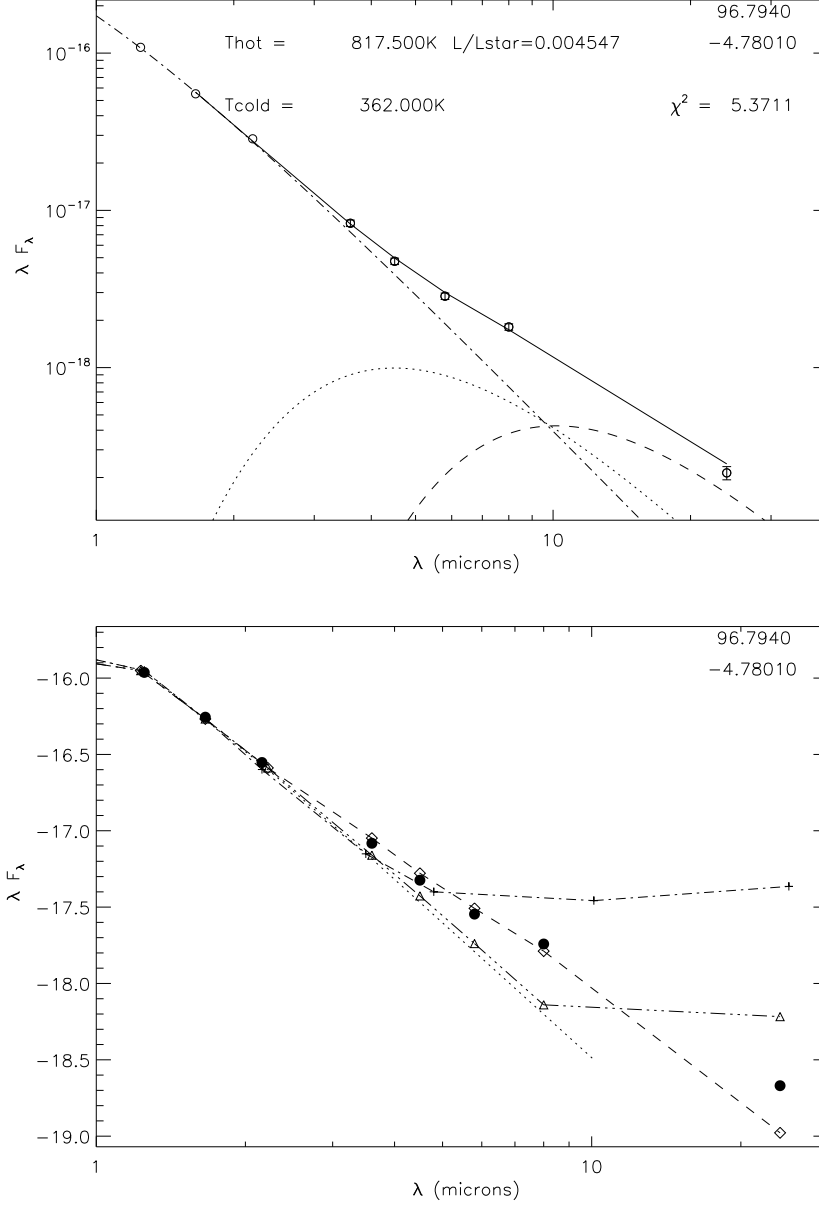


Fig. 10.— SED models for ID 18566. (top) Blackbody fits to the SED of ID 18566, using a stellar blackbody (dot-dashed line), a hot dust component (dotted line), and a warm dust component (dashed line). The blackbody fits reveal a population of hot/warm dust. The disk has a fractional luminosity characteristic of luminous debris disks. (bottom) SED modeling of the star compared to a transition disk model (dashed-dotted line/crosses), a terrestrial zone debris disk model (dashed line/diamonds), and a cold debris disk model (dashed-three dots/triangles). The stellar photosphere is shown for reference (dotted line).

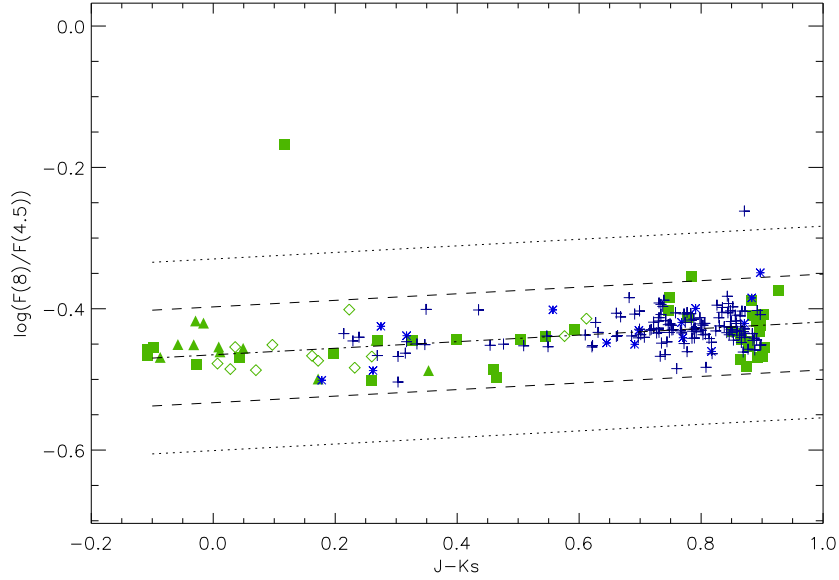


Fig. 11.— The  $8\ \mu m$  to  $4.5\ \mu m$  flux ratio as a function of  $J-K_s$  used to identify NGC 2232 cluster stars with IRAC excesses. The dash-dotted line shows the linear least-squares fit to the flux ratios (rms residuals are  $\sim 3.92\%$ ). Dashed lines identify the  $4\sigma$  limit beyond which we identify excess sources. The dotted lines show the  $8\sigma$  limits. IR excess sources are identified as those with flux ratios greater than  $4\sigma$  from the photosphere. Four stars in NGC 2232 have flux ratios consistent with IRAC excesses from warm dust. From left to right, these sources are ID 18566 ( $J-K_s \approx 0.1$ ), ID 18613 ( $J-K_s \approx 0.8$ ), ID 6540 ( $J-K_s \approx 0.85$ ), and ID 9220 ( $J-K_s \approx 0.9$ ).

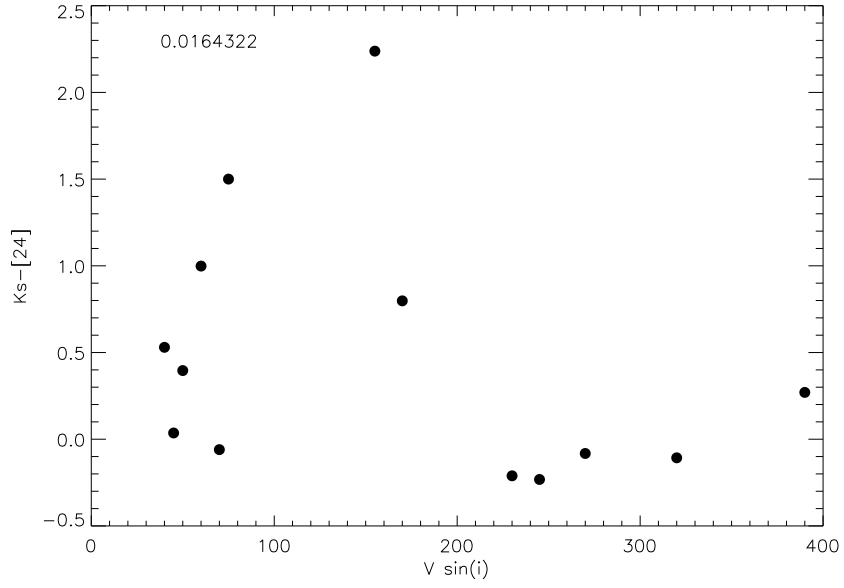


Fig. 12.—  $V \sin i$  ( $\text{km s}^{-1}$ ) vs.  $K_s - [24]$  for B1–A3 stars in NGC 2232. The probability that  $K_s - [24]$  is uncorrelated with  $V \sin i$  is  $\sim 1.6\%$ . Thus, the data show that slower rotators typically have stronger IR excesses.

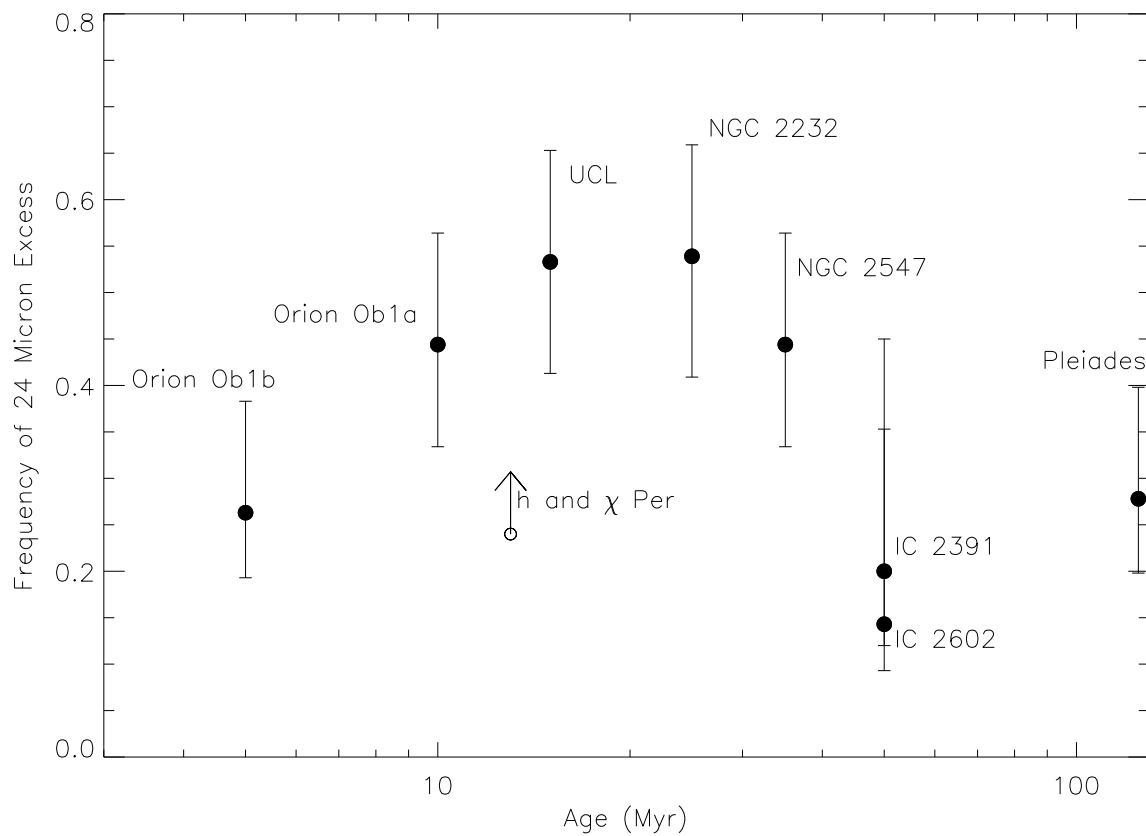


Fig. 13.— Frequency of 24  $\mu m$  excess vs. age for B and A stars in several open clusters studied by Spitzer. The frequency of debris emission apparently *increases* from 5 Myr to  $\approx$  10-25 Myr before declining after  $\approx$  40 Myr.

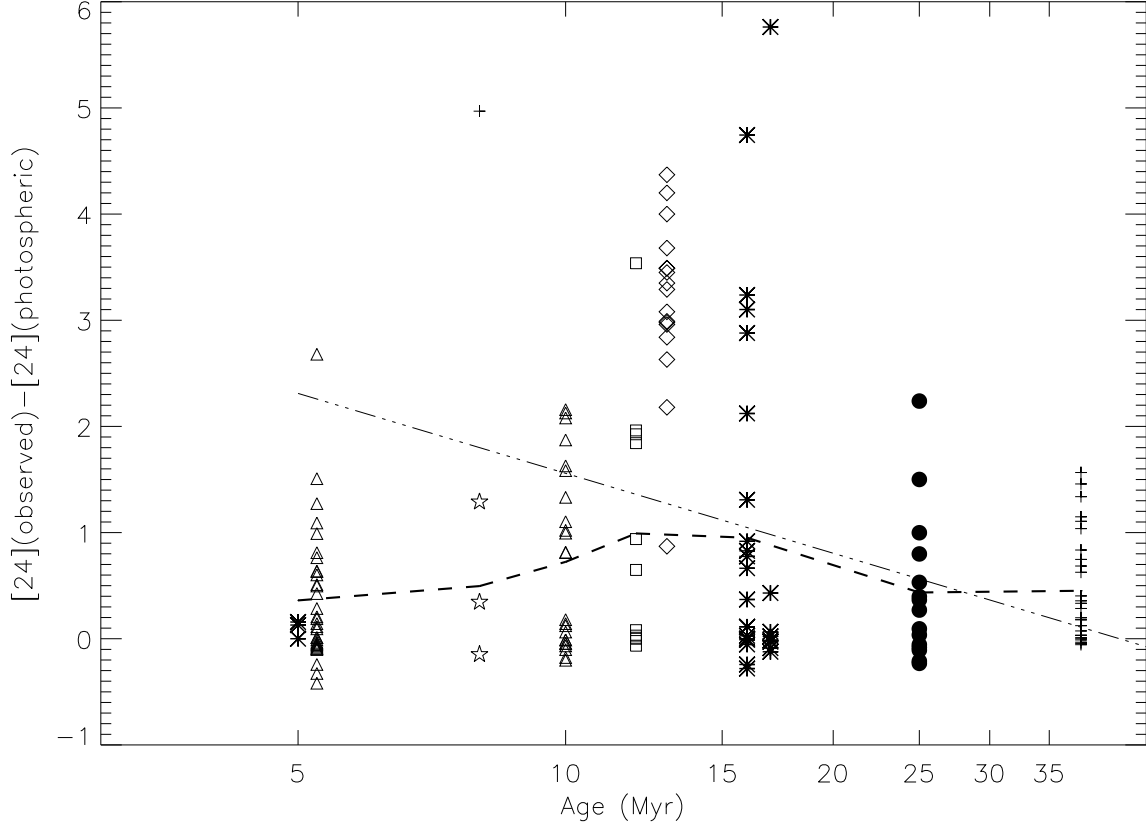


Fig. 14.— Level of  $24\ \mu\text{m}$  excess around BAF stars vs. time for 5–40 Myr old clusters. We include Orion Ob1a and b (10 and 5 Myr; triangles),  $\eta$  Cha (8 Myr; stars), the  $\beta$  Pic Moving Group (12 Myr; squares), h and  $\chi$  Persei (13 Myr; diamonds), Sco-Cen (5, 16, and 17 Myr; asterisks), NGC 2232 (25 Myr filled circles), and NGC 2547 (38 Myr; small crosses). HR 4796A, from Low et al. (2005) is also shown as a cross at  $t \sim 8$  Myr and  $[24] - [24]_{\text{phot}} \sim 5$ . The data are consistent with a rise in debris emission from 5 Myr to 10 Myr, a peak from  $\sim 10$  Myr to 20 Myr. For stars older than  $\approx 40$  Myr, the distribution of  $24\ \mu\text{m}$  luminosity defines an envelope which is consistent with a  $t^{-1}$  decline (Rieke et al. 2005). The dashed line shows the mean excess. Predictions for the decline in emission from a steady-state collisional evolution model (dash-three dots) follow a  $t^{-1}$  decline.